nature

https://doi.org/10.1038/s41586-021-03361-1

Accelerated Article Preview

SARS-CoV-2 spike D614G change enhances replication and transmission

Received: 15 October 2020

Accepted: 16 February 2021

Accelerated Article Preview Published online 26 February 2021

Cite this article as: Zhou, B. et al. SARS-CoV-2 spike D614G change enhances replication and transmission. *Nature* https://doi.org/10.1038/s41586-021-03361-1 (2021).

Bin Zhou, Tran Thi Nhu Thao, Donata Hoffmann, Adriano Taddeo, Nadine Ebert, Fabien Labroussaa, Anne Pohlmann, Jacqueline King, Silvio Steiner, Jenna N. Kelly, Jasmine Portmann, Nico Joel Halwe, Lorenz Ulrich, Bettina Salome Trüeb, Xiaoyu Fan, Bernd Hoffmann, Li Wang, Lisa Thomann, Xudong Lin, Hanspeter Stalder, Berta Pozzi, Simone de Brot, Nannan Jiang, Dan Cui, Jaber Hossain, Malania Wilson, Matthew Keller, Thomas J. Stark, John R. Barnes, Ronald Dijkman, Joerg Jores, Charaf Benarafa, David E. Wentworth, Volker Thiel & Martin Beer

Article

SARS-CoV-2 spike D614G change enhances replication and transmission

https://doi.org/10.1038/s41586-021-03361-1

Received: 15 October 2020

Accepted: 16 February 2021

Published online: 26 February 2021

Bin Zhou[1,12], Tran Thi Nhu Thao[2,3,4,12], Donata Hoffmann[5,12], Adriano Taddeo[2,3,12], Nadine Ebert[2,3], Fabien Labroussaa[3,6], Anne Pohlmann[5], Jacqueline King[5], Silvio Steiner[2,3,4], Jenna N. Kelly[2,3], Jasmine Portmann[2,3], Nico Joel Halwe[5], Lorenz Ulrich[5], Bettina Salome Trüeb[3,6], Xiaoyu Fan[1], Bernd Hoffmann[5], Li Wang[1], Lisa Thomann[2,3], Xudong Lin[7], Hanspeter Stalder[2,3], Berta Pozzi[8], Simone de Brot[9], Nannan Jiang[10], Dan Cui[7], Jaber Hossain[1], Malania Wilson[1], Matthew Keller[1], Thomas J. Stark[1], John R. Barnes[1], Ronald Dijkman[2,3,11], Joerg Jores[3,6], Charaf Benarafa[2,3,13]✉, David E. Wentworth[1,13]✉, Volker Thiel[2,3,13]✉ & Martin Beer[5,13]✉

During the evolution of SARS-CoV-2 in humans a D614G substitution in the spike (S) protein emerged and became the predominant circulating variant (S-614G) of the COVID-19 pandemic[1]. However, whether the increasing prevalence of the S-614G variant represents a fitness advantage that improves replication and/or transmission in humans or is merely due to founder effects remains elusive. Here, we generated isogenic SARS-CoV-2 variants and demonstrate that the S-614G variant has (i) enhanced binding to human host cell surface receptor angiotensin-converting enzyme 2 (ACE2), (ii) increased replication in primary human bronchial and nasal airway epithelial cultures as well as in a novel human ACE2 knock-in mouse model, and (iii) markedly increased replication and transmissibility in hamster and ferret models of SARS-CoV-2 infection. Collectively, our data show that while the S-614G substitution results in subtle increases in binding and replication *in vitro*, it provides a real competitive advantage *in vivo*, particularly during the transmission bottle neck, providing an explanation for the global predominance of S-614G variant among the SARS-CoV-2 viruses currently circulating.

In late 2019, severe acute respiratory syndrome coronavirus 2 (SARS-CoV-2) emerged in Wuhan, Hubei province, China[2,3] and rapidly developed into the COVID-19 pandemic. By December 2020, 70 million cases and 1.5 million deaths have been confirmed[4]. In vulnerable groups of people, SARS-CoV-2 causes a life-threatening pneumonia[5]. Cell entry of SARS-CoV-2 is dependent on the interaction of the spike glycoprotein (S) and ACE2[3,6]. S, a homotrimeric class I fusion protein consists of two subunits S1 and S2, separated by a protease cleavage site. S1 forms a globular head and is essential for receptor binding, while S2 mediates fusion of the viral envelope with host cell membranes. During entry, the receptor-binding domain (RBD) within the S1 subunit binds ACE2, generating conformational changes in the S2 subunit, facilitating virus internalization[7,8]. S-D614G, a protein variant containing a substitution in the S protein outside of the RBD, is thought to cause a conformational change, improving ACE2 binding and increasing the probability of infection[1,9].

As the pandemic progressed, the SARS-CoV-2 S-614G variant rapidly superseded the parental S-614D variant in frequency to become globally dominant. Such a shift in genotype frequency might be caused by a founder effect following introduction into a highly interconnected population. However, the S-614G variant may confer a fitness advantage compared to S-614D. However, some studies suggest the S-614G substitution may confer a fitness advantage by improving entry[8,9]. To address the role that the S-D614G substitution has played in the dissemination and predominance of this SARS-CoV-2 variant during the COVID-19 pandemic, we characterized S protein binding to human ACE2 (hACE2) and replication kinetics *in vitro* and evaluated infection and transmission dynamics *in vivo* using three different animal models. The data show that the S-D614G substitution confers increased binding to the hACE2 receptor and increased replication in primary human airway epithelial cultures. Moreover, comparison of recombinant isogenic SARS-CoV-2 variants demonstrates that S-614G substitution provides competitive advantage in a hACE2 knock-in mouse model, and markedly increases replication and transmission in Syrian hamster and ferret models. To address the role that the S-D614G substitution has played in the dissemination and predominance of this SARS-CoV-2 variant during the COVID-19 pandemic, we characterized S protein binding to human ACE2 (hACE2) and replication kinetics *in vitro* and evaluated infection and transmission dynamics *in vivo* using three different animal models.

[1]CDC COVID-19 Response, Centers for Disease Control and Prevention, Atlanta, Georgia, United States of America. [2]Institute of Virology and Immunology (IVI), Bern and Mittelhäusern, Bern, Switzerland. [3]Department of Infectious Diseases and Pathobiology, Vetsuisse Faculty, University of Bern, Bern, Switzerland. [4]Graduate School for Biomedical Science, University of Bern, Bern, Switzerland. [5]Institute of Diagnostic Virology, Friedrich-Loeffler-Institut, Greifswald-Insel Riems, Germany. [6]Institute of Veterinary Bacteriology, Vetsuisse Faculty, University of Bern, Bern, Switzerland. [7]Battelle Memorial Institute, Atlanta, Georgia, United States of America. [8]Institute of Cell Biology, University of Bern, Bern, Switzerland. [9]COMPATH, Institute of Animal Pathology, University of Bern, Bern, Switzerland. [10]Oak Ridge Institute for Science and Education, Oak Ridge, Tennessee, United States of America. [11]Institute for Infectious Diseases, University of Bern, Bern, Switzerland. [12]These authors contributed equally: Bin Zhou, Tran Thi Nhu Thao, Donata Hoffmann, Adriano Taddeo. [13]These authors jointly supervised this work: Charaf Benarafa, David E. Wentworth, Volker Thiel, Martin Beer. ✉e-mail: charaf.benarafa@vetsuisse.unibe.ch; dwentworth@cdc.gov; volker.thiel@vetsuisse.unibe.ch; martin.beer@fli.de

The data show that the S-D614G substitution confers increased binding to the hACE2 receptor and increased replication in primary human airway epithelial cultures. Moreover, comparison of recombinant isogenic SARS-CoV-2 variants demonstrates that S-614G substitution provides competitive advantage in a hACE2 knock-in mouse model, and markedly increases replication and transmission in Syrian hamster and ferret models.

SARS-CoV-2 S-614G binds to hACE2 more efficiently

To measure the effects of the S-D614G substitution, binding of S1 domain monomers to hACE2, were first quantified using bio-layer interferometry. Both S1 proteins with 614D or 614G (S1-614D and S1-614G, respectively) bind efficiently to hACE2; however, S1-614G showed about 2-fold higher affinity than S1-614D (Figure 1a; Supplementary Table 2). Similarly, higher affinity to hACE2 was observed for the S-614G protein when full-length monomeric spike was used (Extended Data Figure 1a; Supplementary Table 2). The S-D614G substitution also resulted in enhanced S1 binding to hACE2 exogenously expressed in Baby Hamster Kidney cells (BHK-hACE2) (Figure 1b, Extended Data Figure 1b). Binding of polyhistidine-tagged S1-614D or S1-614G proteins to BHK-hACE2 cells showed more S1-614G bound to BHK-hACE2 cells than S1-614D by flow cytometry (Figure 1b, Extended Data Figure 1b). When using homo-dimeric recombinant constructs composed of S1 attached to an IgG carboxyl-terminus, a more striking effect was observed in the increased binding of the S1-614G protein to the BHK-hACE2 cell (Figure 1b, Extended Data Figure 1b).

Increased replication of SARS-CoV-2$^{S\text{-}614G}$ virus in primary human epithelial cells

To assess the impact of S-614G in the context of virus infection we generated an isogenic D614G virus pair using our SARS-CoV-2 reverse genetics system[10]. The molecular clone based on Wuhan-Hu-1 isolate is representative of the S-614D variant (SARS-CoV-2$^{S\text{-}614D}$)[10,11]. The sequence of the isogenic S-614G variant was engineered with an A to G transition at position 23,403 to encode a glycine at S protein position 614. The identity of the resulting recombinant SARS-CoV-2$^{S\text{-}614G}$ variant was confirmed by genomic next-generation sequencing (NGS) of virus stock (p1) used in subsequent experiments. Replication kinetics of SARS-CoV-2$^{S\text{-}614D}$ and SARS-CoV-2$^{S\text{-}614G}$ in Vero E6 cells differed marginally (Figure 1c). We assessed replication kinetics in primary human nasal epithelial (hNE) and primary normal human bronchial epithelial (NhBE) cultures grown under air-liquid interface conditions that resemble the pseudostratified epithelial lining of the human respiratory epithelium. No significant difference in the primary hNE cells following infection of SARS-CoV-2$^{S\text{-}614D}$ or SARS-CoV-2$^{S\text{-}614G}$ was observed at 33 °C, the temperature of the nasal epithelium (Figure 1c). In contrast, SARS-CoV-2$^{S\text{-}614G}$ displayed elevated titers in primary NhBE cells at 33 °C, 37 °C, and 39 °C, mimicking temperatures of the upper respiratory tract, lower respiratory tract, or fever, respectively (Figure 1d). Infection kinetics of NhBE cells with natural isolates SARS-CoV-2/USA-WA1/2020 (USA-WA1, S-614D) or SARS-CoV-2/Massachusetts/VPT1/2020 (MA/VPT1, S-614G) showed a more subtle advantage for the S-614G variant at 37 °C and 39 °C (Extended Data Figure 1c). To refine this analysis, we performed competition experiments infecting hNE and NhBE cultures with a mixture of both SARS-CoV-2$^{S\text{-}614D}$ and SARS-CoV-2$^{S\text{-}614G}$, at defined ratios. In both primary human respiratory culture systems, the ratio of 614G:614D shifted in favor of SARS-CoV-2$^{S\text{-}614G}$ during five or eight days of infection (Figure 1e, f; Extended Data Figures 1d, e, 2a, b). Collectively, these results show that the D614G change in the S protein is associated with enhanced hACE2 binding and increased replication in primary human airway epithelial models of SARS-CoV-2 infection.

Increased replication of SARS-CoV-2$^{S\text{-}614G}$ in hACE2 knock-in mice

Mice do not support efficient replication of SARS-CoV-2 unless they are genetically engineered to express hACE2[12,13]. To evaluate the relative fitness of the SARS-CoV-2$^{S\text{-}614G}$ variant *in vivo*, we generated knock-in mice expressing *hACE2* under the endogenous regulatory elements of the mouse *Ace2* gene (hACE2-KI, Extended Data Figure 3a). Eight heterozygous female mice were inoculated intranasally (i.n.) in a competition experiment with an equal mixture of both viruses, SARS-CoV-2$^{S\text{-}614D}$ and SARS-CoV-2$^{S\text{-}614G}$, by pooling $1x10^5$ plaque-forming units (PFU) of each variant (Figure 2a). Viral RNA loads were monitored in oropharyngeal swabs (daily), and various tissues (at days 2 and 4 post inoculation p.i) by real-time PCR. No significant body weight loss in hACE2-KI mice up to day 4 p.i. were observed (Extended Data Figure 3b). Longitudinal analysis of oropharyngeal swabs revealed efficient virus replication in the upper respiratory tract of hACE2-KI mice relative to wild-type mice (Figure 2b). Accordingly, tissue samples collected at days 2 and 4 p.i. revealed high viral loads in the nasal conchae, lungs, and olfactory bulbs and lower levels in the brain (Extended Data Figure 3c, d). Low to undetectable levels of viral RNA was observed in spleen, small intestine, kidneys, and feces (data not shown). No overt pathological lesions were found in the lungs at days 2 and 4 p.i. (Supplementary Table 3, 4). NGS of the oropharyngeal swabs revealed a net advantage for SARS-CoV-2$^{S\text{-}614G}$ over SARS-CoV-2$^{S\text{-}614D}$ in most animals and time points (Figure 2c; Extended Data Figure 3e, f). In the organs, a similar replication advantage was found for SARS-CoV-2$^{S\text{-}614G}$ (Figure 2d). Collectively, these results demonstrate increased replication of SARS-CoV-2$^{S\text{-}614G}$ in a mouse model that expresses the authentic human receptor (*hACE2*).

SARS-CoV-2$^{S\text{-}614G}$ displays increased replication and transmissibility in hamsters and ferrets

Hamsters are highly susceptible to SARS-CoV-2 infection and develop disease that closely resembles pan-respiratory, moderate to severe COVID-19 disease in humans[14–16]. To examine the replication kinetics of the S-614 variants using the hamster model, seven hamsters were intranasally inoculated with either SARS-CoV-2$^{S\text{-}614D}$ or SARS-CoV-2$^{S\text{-}614G}$ ($1x10^{5.1}$ $TCID_{50}$/animal, and $10^{4.5}$ $TCID_{50}$/animal, respectively, calculated from back titration of the inoculum) and were monitored for four consecutive days. No marked differences in body weights, titers of shed virus, or viral loads in respiratory tract tissue were observed between the two groups in the acute phase (Extended Data Figure 4c-e). For both S-614 variants, highest genome loads were found in the nasal conchae, followed by pulmonary tissue (Extended Data Figure 4e). These observations suggest that in the case of SARS-CoV-2$^{S\text{-}614D}$ or SARS-CoV-2$^{S\text{-}614G}$ infections, the S-D614G substitution does not have strong impact on clinical outcomes or a detectable replication advantage in the hamster model.

An *in vivo* competition experiment was therefore setup to better elucidate potential replication and/or transmission differences between the S-614 variants. Six donor Syrian hamsters were intranasally inoculated with 1:1 mixture (based on infectious PFU titer) of SARS-CoV-2$^{S\text{-}614D}$ and SARS-CoV-2$^{S\text{-}614G}$ in direct "one-to-one" transmission experiments. The RNA ratio of the two variants within the inoculum was later confirmed using NGS and absolute quantification using digital droplet PCR with allele-specific locked nucleic acid (LNA) probes (Figure 3). At 24 hours after inoculation, each inoculated hamster was cohoused with one naive hamster. Viral RNA load in daily nasal washings, changes in body weight and clinical signs, agreed with previous data[14–16] (Extended Data Figure 4a, b). NGS of the viral RNA sequence composition of nasal washings revealed a prominent shift towards SARS-CoV-2S-614G within 48 hours post inoculation (Figure 3, Extended Data Figure 4f, g). Transmission efficiency was 100%, and analysis of the RNA sequence composition showed that the SARS-CoV-2$^{S\text{-}614G}$ variant represented >90% of

the viral RNA in the contact animals (Figure 3). In summary, hamsters inoculated with an equal ratio of SARS-CoV-$2^{S\text{-}614D}$ and SARS-CoV-$2^{S\text{-}614G}$ transmit 24h post inoculation primarily SARS-CoV-$2^{S\text{-}614G}$.

We further investigated the competitive advantage of D614G in ferrets, a good transmission model[17] in which SARS-CoV-2 replicates primarily within the upper respiratory tract, resembling mild human infections. Six animals were intranasally inoculated with 1:1 mixture (based on infectious PFU titer) of SARS-CoV-$2^{S\text{-}614D}$ and SARS-CoV-$2^{S\text{-}614G}$ in direct "one-to-one" transmission experiments. For all six inoculated ferrets SARS-CoV-2-infection could be confirmed, and body weight changes and viral RNA loads in nasal washings (Figure 4, Extended Data Figure 5a, b) reflected published data[17,18]. In five of the six inoculated ferrets, SARS-CoV-$2^{S\text{-}614G}$ became the dominant variant (Figure 4; Extended Data Figure 5c, d). Also, SARS-CoV-2 transmission occurred in four of the six ferret pairs. In each pair with successful transmission, the S-614G variant prevailed over S-614D (Figure 4). All NGS data of the ferret samples were also retested by absolute quantification using allele-specific locked nucleic acid (LNA) probes and digital PCR analysis. Notably, the inoculated ferret from pair one, where SARS-CoV-$2^{S\text{-}614D}$ predominated the viral population, did not transmit virus to the contact despite a high peak viral genome load of more than 10 million copies per ml. In contrast, the lack of transmission in pair 4 where SARS-CoV-$2^{S\text{-}614G}$ became the dominant variant is connected to peak viral loads of below 500,000 genome copies per ml (Figure 4). In summary, the competition experiment in ferrets revealed that the SARS-CoV-$2^{S\text{-}614G}$ variant preferentially infected and replicated in five out of six inoculated animals, and transmission events succeeded exclusively with the SARS-CoV-$2^{S\text{-}614G}$ variant.

Discussion

SARS-CoV-2 evolution in humans is proposed to be a non-deterministic process and virus diversification results mainly from random genetic drift, suggesting no strong selective pressure in its adaptation to humans[19]. However, since the emergence of the S-D614G in early 2020, the SARS-CoV-2 S-614G variant has become globally prevalent[1]. Both founder effect and spike protein structural changes have been proposed as driving forces establishing the S-614G prevalence. Previous structural studies and the use of pseudotyped viruses have suggested that the S-614G variant may confer increased infectivity, as a result of increased "open" RBD conformation for receptor binding or increased S stability[1,9]. In contrast to studies that used recombinant trimeric S, we used a reductionist approach to eliminate complications due to "open" or "closed" RBD conformations in trimeric S. We found the S1 or the monomeric S ectodomain with D614G substitution had increased affinity to hACE2, which may be another mechanism underlying the increased replication and transmission of the SARS-CoV-2 D614G variant.

Studies employing isogenic SARS-CoV-2 D614G variants to assess the phenotype in the context of a SARS-CoV-2 infection were only recently reported[20,21]. Both demonstrated that SARS-CoV-2 S-614G variant increased replication *in vitro* and one observed earlier transmission in a hamster model. We extended these studies by exploiting various *in vitro* and *in vivo* infection models of SARS-CoV-2, including primary NhBE and hNE cultures, a novel hACE2 knock-in mouse model, a hamster model, and a ferret model. Importantly, throughout these experimental systems, we consistently observed increased replicative fitness of SARS-CoV-$2^{S\text{-}614G}$ over SARS-CoV-$2^{S\text{-}614D}$ by applying NGS techniques and allele-specific absolute quantification for confirmation. The advantage provided by the D614G change becomes most prominent in competition and transmission experiments in hamsters and ferrets and must therefore be considered as a driving force leading to the global dominance of the SARS-CoV-2 614G variant.

Our data also agree with reported functional changes conferred by the D614G substitution in the S protein[1] and infections studies using pseudotyped viruses demonstrating increased infection[9,22]. Although our studies establish a phenotype of increased replication and transmission of the SARS-CoV-2 S-614G variant, there is no evidence for a phenotypic change in pathogenicity in animal models. This is important because infection with the SARS-CoV-2 S-614G variant is not associated with the development of severe COVID-19 in humans[1].

The ongoing pandemic will likely give rise to additional SARS-CoV-2 variants that may display phenotypic changes and further adaptations to humans or animal reservoirs like minks. The ability to rapidly identify emerging variants using genomics, reconstructing emerging virus variants, and assessing their phenotypes *in vitro* and *in vivo* will allow rapid response to their emergence with appropriate countermeasures. The novel mouse model based on hACE2 expression under the endogenous regulatory elements of the mouse *Ace2* gene is a valuable tool and will complement existing animal models of SARS-CoV-2 infection. Similarly, to demonstrate increased replication and transmissibility of SARS-CoV-$2^{S\text{-}614G}$, the phenotypic assessment of future pandemic variants will likely require several complementing animal models that together reflect aspects of SARS-CoV-2 replication, transmission, and pathogenicity in humans.

Online content

Any methods, additional references, Nature Research reporting summaries, source data, extended data, supplementary information, acknowledgements, peer review information; details of author contributions and competing interests; and statements of data and code availability are available at https://doi.org/10.1038/s41586-021-03361-1.

1. Korber, B. et al. Tracking Changes in SARS-CoV-2 Spike: Evidence that D614G Increases Infectivity of the COVID-19 Virus. *Cell* **182**, 812-827.e19 (2020).
2. Zhu, N. et al. A Novel Coronavirus from Patients with Pneumonia in China, 2019. *N Engl J Med* **382**, 727-733 (2020).
3. Zhou, P. et al. A pneumonia outbreak associated with a new coronavirus of probable bat origin. *Nature* **579**, 270-273 (2020).
4. ECDC. (2020).
5. Huang, C. et al. Clinical features of patients infected with 2019 novel coronavirus in Wuhan, China. *Lancet* **395**, 497-506 (2020).
6. Letko, M., Marzi, A. & Munster, V. Functional assessment of cell entry and receptor usage for SARS-CoV-2 and other lineage B betacoronaviruses. Nature *Microbiology* **5**, 562-569 (2020).
7. Wrapp, D. et al. Cryo-EM structure of the 2019-nCoV spike in the prefusion conformation. *Science* **367**, 1260-1263 (2020).
8. Hoffmann, M. et al. SARS-CoV-2 Cell Entry Depends on ACE2 and TMPRSS2 and Is Blocked by a Clinically Proven Protease Inhibitor. *Cell* **181**, 271-280.e8 (2020).
9. Yurkovetskiy, L. et al. Structural and Functional Analysis of the D614G SARS-CoV-2 Spike Protein Variant. Cell (2020).
10. Thi Nhu Thao, T. et al. Rapid reconstruction of SARS-CoV-2 using a synthetic genomics platform. *Nature* **582**, 561-565 (2020).
11. Wu, F. et al. A new coronavirus associated with human respiratory disease in China. *Nature* **579**, 265-269 (2020).
12. Bao, L. et al. The pathogenicity of SARS-CoV-2 in hACE2 transgenic mice. *Nature* **583**, 830-833 (2020).
13. Jiang, R.D. et al. Pathogenesis of SARS-CoV-2 in Transgenic Mice Expressing Human Angiotensin-Converting Enzyme 2. *Cell* **182**, 50-58 e8 (2020).
14. Sia, S.F. et al. Pathogenesis and transmission of SARS-CoV-2 in golden hamsters. *Nature* **583**, 834-838 (2020).
15. Osterrieder, N. et al. Age-Dependent Progression of SARS-CoV-2 Infection in Syrian Hamsters. *Viruses* **12** (2020).
16. Imai, M. et al. Syrian hamsters as a small animal model for SARS-CoV-2 infection and countermeasure development. *Proc Natl Acad Sci U S A* **117**, 16587-16595 (2020).
17. Richard, M. et al. SARS-CoV-2 is transmitted via contact and via the air between ferrets. *Nat Commun* **11**, 3496 (2020).
18. Kim, Y.I. et al. Infection and Rapid Transmission of SARS-CoV-2 in Ferrets. *Cell Host Microbe* **27**, 704-709.e2 (2020).
19. Alouane, T. et al. Genomic Diversity and Hotspot Mutations in 30,983 SARS-CoV-2 Genomes: Moving Toward a Universal Vaccine for the "Confined Virus"? *Pathogens* **9** (2020).
20. Plante, J.A. et al. Spike mutation D614G alters SARS-CoV-2 fitness. *Nature* (2020).
21. Hou, Y.J. et al. SARS-CoV-2 D614G variant exhibits efficient replication ex vivo and transmission in vivo. *Science* (2020).
22. Li, Q. et al. The Impact of Mutations in SARS-CoV-2 Spike on Viral Infectivity and Antigenicity. *Cell* **182**, 1284-1294 e9 (2020).

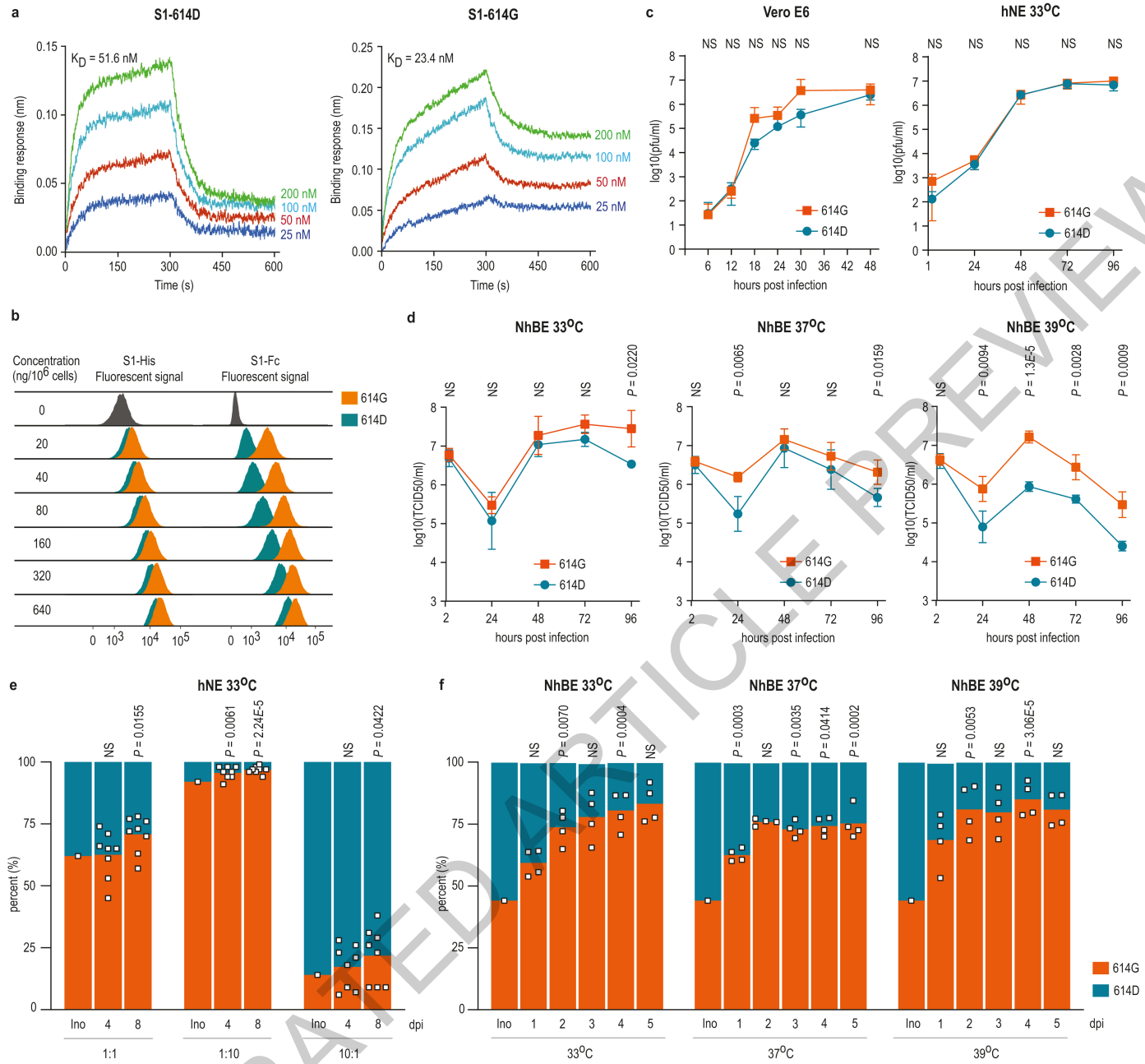

Fig. 1 | In vitro characterization of S1 proteins and recombinant SARS-CoV-2$^{S\text{-}614D}$ and SARS-CoV-2$^{S\text{-}614G}$ viruses. (a) Affinity between S1 and hACE2 determined by Bio-layer interferometry. Fc-tagged hACE2 protein was loaded onto surface of AHC biosensors. Association was conducted using S1-614D or S1-614G protein followed by dissociation. Data represent three biological replicates. **(b)** Binding of polyhistidine-tagged or Fc-tagged S1 to BHK-hACE2 cells is shown as peaks of fluorescence detected by flow cytometry. **(c)** Replication kinetics of recombinant viruses in (left) Vero E6 at 37°C and (right) hNE at 33°C. Supernatant was collected at indicated time points and titrated by plaque assay. **(d)** Replication kinetics of recombinant viruses in NhBE at 33°C (left), 37°C (middle) and 39°C (right). Supernatant was collected daily and titrated by TCID50 assay. **(c-d)** Data represent the mean ± s.d. of three biological replicates (Vero E6) or four technical replicates (hNE and NhBE). Statistical significance was determined by two-sided unpaired Student's *t*-test without adjustments for multiple comparisons. **(c-d)** *P* values NS, *P* > *0.05*. **(e-f)** Competition assay of recombinant viruses in hNE at 33°C and NhBE at 33°C, 37°C and 39°C. The inoculum was prepared by mixing two viruses and used for infection of hNE (1:1, 1:10, and 10:1 PFU ratios, 8 technical replicates each) and NhBE (1:1 PFU ratio, 4 technical replicates each). Apical wash and supernatant were collected daily, and extracted RNA was used for NGS. Bar graphs show percentage of sequence reads encoding either S-614D or S-614G. Each square represents individual data point in competition experiments in hNE and NhBE. For each time point, a linear regression model was generated based on the sequencing read counts for S-614D and S-614G, and P values were calculated for the group (variant) coeffiecient. *P* values: NS, *P* > 0.05. dpi: days post infection.

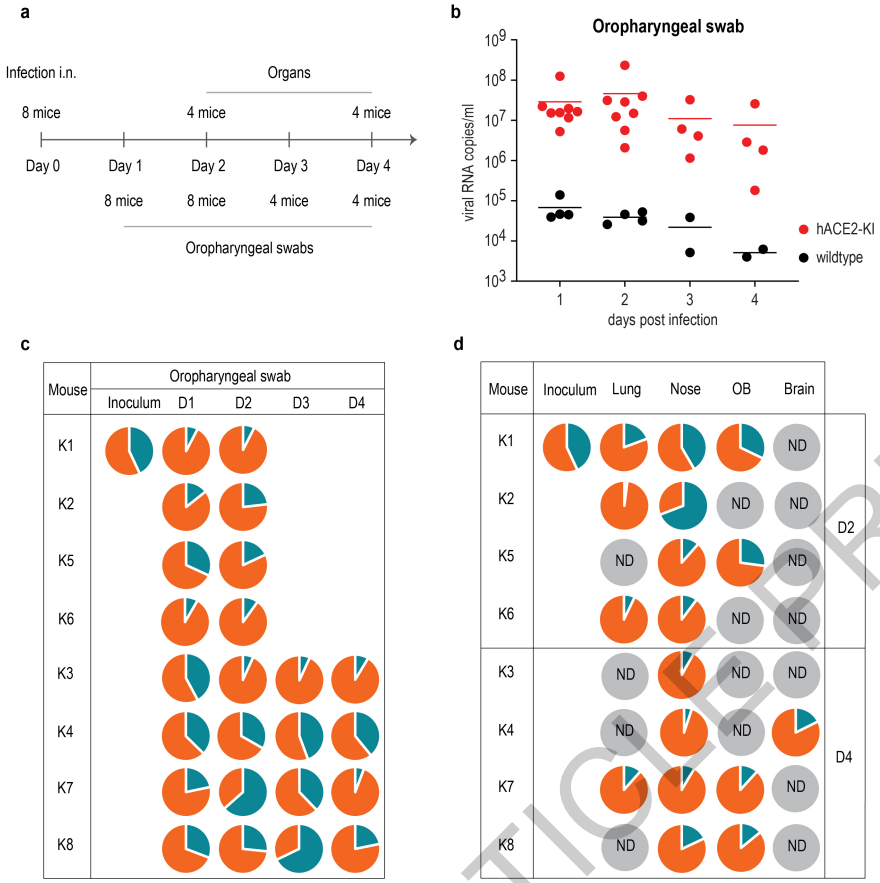

Fig. 2 | Replication of SARS-CoV-2$^{S\text{-}614D}$ and SARS-CoV-2$^{S\text{-}614G}$ viruses in hACE2 knock-in mice. (**a**) Experimental scheme for infection of hACE2-KI mice intranasally (i.n) infected recombinant SARS-CoV-2$^{S\text{-}614D}$ and SARS-CoV-2$^{S\text{-}614G}$ viruses. Oropharyngeal swabs were sampled daily and tissue samples were analyzed in sub-groups of 4 mice at 2 and 4 days post infection in two independent experiments. (**b**) Quantitative RT-PCR analysis of oropharyngeal swabs of inoculated hACE2-KI and wild-type mice. (**c,d**) Pie chart representation of mean frequencies of A or G nucleotide at position 23,403 corresponding to SARS-CoV-2$^{S\text{-}614D}$ and SARS-CoV-2$^{S\text{-}614G}$, respectively. Each pie chart illustrates the ratio of A/G detected from individual oropharyngeal swab samples (c) and tissues (d) at indicated time post infection. OB, olfactory bulb; ND, not detected; D: day.

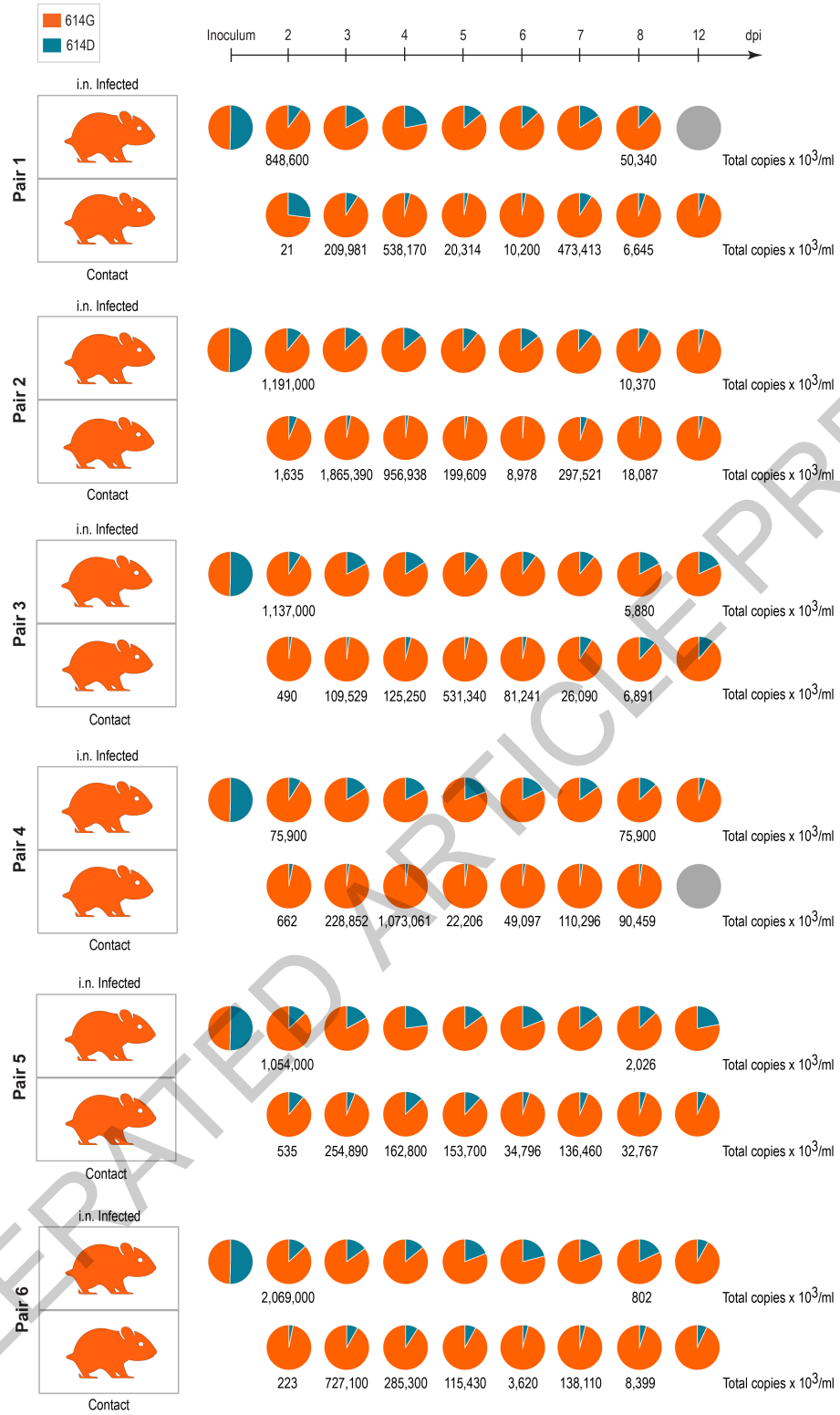

Fig. 3 | Replication and transmission of SARS-CoV-2$^{S\text{-}614D}$ and SARS-CoV-2$^{S\text{-}614G}$ viruses in Syrian hamsters. Transmission of SARS-CoV-2$^{S\text{-}614D}$ and $^{S\text{-}614G}$ variant by hamsters in a pairwise one-by-one setup with direct contact of donor and cohoused contact hamsters is illustrated. Samples of nasal washings were taken daily between days 2 to 8 post infection (dpi) and finally at 12 dpi and were analyzed. Pie chart representation of fraction of A or G nucleotide at position 23,403 corresponding to SARS-CoV-2$^{S\text{-}614D}$ and SARS-CoV-2$^{S\text{-}614G}$, respectively, measured by NGS of amplicons. Genome copies were calculated from RT-qPCR using a standard RNA. Orange coloring of the hamster silhouette refer to detection of G (SARS-CoV-2$^{S\text{-}614G}$), while blue coloring indicates detection of A (SARS-CoV-2$^{S\text{-}614D}$) on most time points. Grey coloring signals no infection detected. i.n: intranasally.

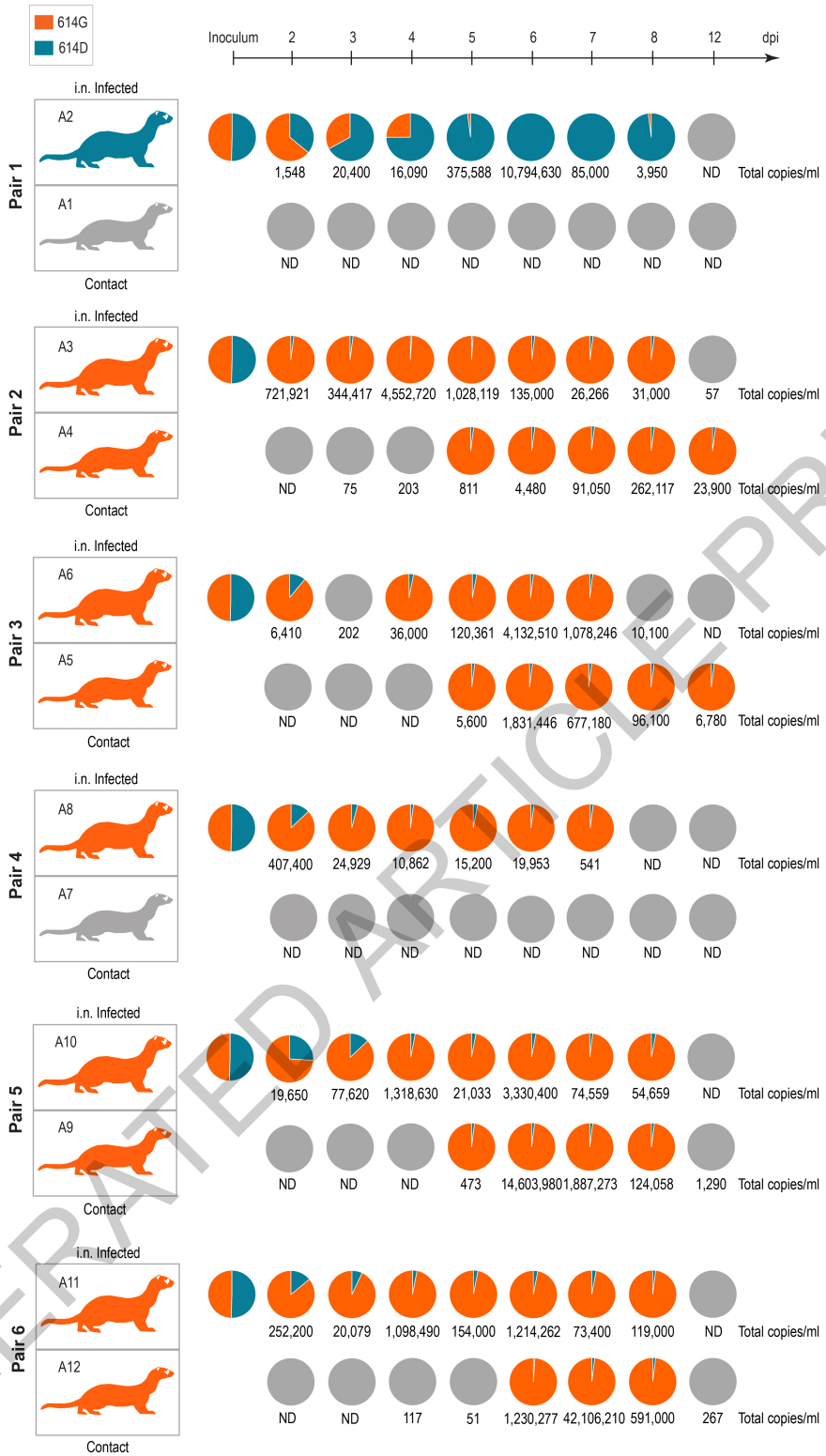

Fig. 4 | Replication and transmission of SARS-CoV-2$^{S\text{-}614D}$ and SARS-CoV-2$^{S\text{-}614G}$ viruses in ferrets. Schematic illustration of the experimental setup with six pairs of donor ferrets cohoused with naïve contact ferrets. Samples of nasal washings were taken daily between days 2 to 8 post infection (dpi) and finally at 12 dpi and were analyzed. Pie chart representation of fraction of A or G nucleotide at position 23,403 corresponding to SARS-CoV-2$^{S\text{-}614D}$ and SARS-CoV-2$^{S\text{-}614G}$, respectively. Each pie chart illustrates the ratio of A/G detected from individual nasal washing samples over time. Orange coloring of the ferret silhouette refer to detection of G (SARS-CoV-2$^{S\text{-}614G}$) on most time points, while blue coloring indicates detection of A (SARS-CoV-2$^{S\text{-}614D}$). Numbers represent total genome copies ml^{-1} and grey coloring signals no infection or viral genome number too low for A/G ratio determination by NGS. ND, not detected; i.n: intranasally.

Methods

Cell and culture conditions

Vero E6 cells (kind gift from Marcel Müller, Charité, Berlin, Germany) were cultured in Dulbecco's modified Eagle's medium (DMEM) supplemented with 10% fetal bovine serum, 1x non-essential amino acids, 100 units ml^{-1} penicillin and 100 µg ml^{-1} streptomycin. Baby Hamster Kidney cells expressing SARS-CoV N protein (BHK-SARS-N)[23] were maintained in minimal essential medium (MEM) supplemented with 5% fetal bovine serum (FBS), 1x non-essential amino acids, 100 units ml^{-1} penicillin and 100 µg ml^{-1} streptomycin, 500 µg ml^{-1} G418 and 10 µg ml^{-1} puromycin. Twenty-four hours before electroporation, BHK-SARS-N cells were treated with 1 µg ml^{-1} doxycyclin to express SARS-CoV N protein. All cell lines were maintained at 37°C and in a 5% CO_2 atmosphere.

Recombinant proteins

The Expi293 Expression system (ThermoFisher Scientific) was used to produce hACE2 and SARS-CoV-2 S proteins. Mammalian expression plasmids were constructed to encode codon-optimized Fc(hIgG1)-tagged hACE2 (hACE2-Fc) or polyhistidine-tagged S (S-614D and S-614G), which contain the full-length ectodomain of S (residues 1-1208, with mutated furin cleavage site and K986P, V987P substitutions). Expi293F cells were transfected with the plasmids and cultured at 37 °C with 8% CO2 at a shaking speed of 125 RPM. The supernatant was harvested on day 5 by centrifugation at 3000 g for 20 minutes at 4 °C. The hACE2-Fc protein was purified using HiTrap Protein A column (GE Life Sciences) in elution buffer containing 0.1 M citric acid, pH 3.0. S proteins were purified using HisTrap FF column (GE Life Sciences) in elution buffer containing 20 mM sodium phosphate, 0.5 M NaCl, 500 mM imidazole, pH 7.4. The eluents were desalted using Zeba spin desalting column 7K MWCO (Thermo Fisher Scientific). The purified proteins were further concentrated on Amicon Ultra Centrifugal Filters 50K NMWL (Sigma-Aldrich) and quantified using Qubit protein assay (ThermoFisher Scientific).

Bio-Layer interferometry (BLI) assay

Affinity between hACE2-Fc and S1-614D (ABclonal, RP01262), S1-614G (ABclonal, RP01287), S-614D or S-614G was evaluated using Octet RED96 instrument (ForteBio) at 30 °C with a shaking speed of 1000 RPM. Following 20 minutes of pre-hydration of Anti-Human Fc-Capture (AHC) biosensors and 1 minute of sensor check, 7.5 nM hACE2-Fc in 10X kinetic buffer (ForteBio) were loaded onto the surface of biosensors for 5 minutes. After 1.5 minutes of baseline equilibration, 5 minutes of association was conducted with 25 to 200 nM of S1-614D, S1-614G, or with 10 to 100 nM of S-614D or S-614G, followed by 5 minutes of dissociation in the same buffer used for baseline equilibration. The data were corrected by subtracting reference sample, 1:1 binding model with global fit was used for determination of affinity constants.

Flow cytometry

A stable clone of BHK cells expressing exogenous hACE2 were pelleted and resuspended in reaction buffer (PBS pH7.4 with 0.02% tween-20 and 4% BSA) at a concentration of 5×10^6 cells/ml. 100 µl/well of the cells were aliquoted into a round-bottom 96-well plate and incubated on ice for at least 5 min. Polyhistidine-tagged S1-614D (40591-V08H) and S1-614G (40591-V08H3) and Fc-tagged S1-614D (40591-v02H) and S1-614G (40591-v02H3) proteins were purchased from Sino Biological Inc. and diluted in reaction buffer on ice. 50 µl of S1 diluents were added into corresponding wells of cells and incubated on ice for 20 min with shaking. After incubation, cells were washed in 200 µl PBST washing solution (PBS pH7.4 with 0.02% tween-20) once and then 100 µl of 1:300 diluted secondary antibody (ThermoFisher Cat # A-21091 for Fc-tag and ThermoFisher Cat # MA1-21315-647 for polyhistidine-tag) was added into each well of cells, mixed, and incubated on ice with shaking for 15 min. After washing twice, cells were resuspended in 200 µl PBST and analyzed using the BD FACSCanto II Flow Cytometer. Data was processed with Flowjo_v10.6.1. Results for BHK control cells (non-hACE2 expressing cells) and gating strategy are provided in Supplementary Figure 1 and Figure 2.

Generation of infectious cDNA clones using TAR cloning and rescue of recombinant viruses

To introduce the 614G mutation to the Spike gene, PCR mutagenesis (Supplementary Table 1) was performed on the pUC57 plasmid containing SARS-CoV-2 fragment 10[10] using Q5® Site-Directed Mutagenesis Kit (New England BioLab). Both D614 and G614 infectious cDNA clones were generated using in-yeast TAR cloning method as described previously[10]. *In vitro* transcription was performed for EagI-cleaved YACs and PCR-amplified SARS-CoV-2 N gene using the T7 RiboMAX Large Scale RNA production system (Promega) as described previously[24]. Transcribed capped mRNA was electroporated into baby hamster kidney (BHK-21) cells expressing SARS-CoV N protein. Electroporated cells were co-cultured with susceptible Vero E6 cells to produce passage 0 (P.0) of the recombinant S-614D and S-614G viruses. Subsequently, progeny viruses were used to infect fresh Vero E6 cells to generate P.1 stocks for downstream experiments.

Virus growth kinetics and plaque assay

Characterization of virus growth kinetics in Vero E6 was performed as described previously[10]. Twenty-four hours before infection, cells were seeded in a 24-well plate at a density of 2.0×10^5 cells per ml. After washing once with PBS, cells were inoculated with viruses at multiplicity of infection (MOI) of 0.01. After 1 h, the inoculum was removed and cells were washed three times with PBS followed by supply with appropriate culture medium.

Plaque forming unit (PFU) per ml of recombinant S-614D and S614-G viruses were determined by plaque assay in a 24-well format. One day before infection, Vero E6 cells were seeded at a density of 2.0×10^5 cells per ml. After washing once with PBS, cells were inoculated with viruses serially diluted in cell culture medium at 1:10 dilution. After 1 h of incubation, inoculum was removed, and cells were washed with PBS and subsequently overlaid with 1:1 mix of 2.4% Avicel and 2X DMEM supplemented with 20% fetal bovine serum, 200 units ml^{-1} penicillin and 200 µg ml^{-1} streptomycin. After 2 days of incubation at 37°C, cells were fixed in 4% (v/v) neutral-buffered formalin before stained with crystal violet.

Statistical significance was determined by two-sided unpaired Student's *t*-test without adjustment for multiple comparisons.

Infection of human nasal and bronchial epithelial cells

Primary human nasal epithelial cultures (hNE; MucilAir™ EP02, Epithelix Sàrl, Genèva, Switzerland) were purchased and handled according to the manufacturer instructions. Normal human bronchial epithelial (NhBE) cells were purchased (Emory University, Atlanta, GA, USA) and cultured according to recommended protocols. The hNE cultures were inoculated with 0.5×10^5 PFU per well, or mixtures of 1:1, 10:1 and 1:10 of SARS-CoV-$2^{S\text{-}614D}$ and SARS-CoV-$2^{S\text{-}614G}$. NhBE cell cultures were inoculated with 1.0×10^5 PFU per well, or with wild type isolates SARS-CoV-2/USA-WA1/2020 (USA-WA1, S-614D) or SARS-CoV-2/Massachusetts/VPT1/2020 (MA/VPT1, S-614G) at 2×10^5 $TCID_{50}$/well. For competition experiments, NhBE cells were inoculated with 1:1 or 9:1 mixed SARS-CoV-$2^{S\text{-}614D}$ and SARS-CoV-$2^{S\text{-}614G}$ at 1×10^5 PFU per well. After incubation at 33 °C for one or two hours, for hNE or NhBE cell cultures respectively, inoculum was removed (or harvested for NhBE as 2h samples), cells were washed, and subsequently incubated, as indicated, at 33 °C, 37 °C, or 39 °C. To monitor viral replication, apical washes were collected every 24 hours. All titers were determined by standard plaque-assay or $TCID_{50}$ on Vero E6 cells.

For competition experiments, viral RNA was extracted from apical washes using the QIAamp 96 Virus QIAcube HT Kit (QIAGEN). The

SARS-CoV-2 genome was amplified using a highly multiplexed tiling PCR reaction based on the ARTIC protocol (https://www.protocols.io/view/ncov-2019-sequencing-protocol-bbmuik6w) with some modification. Briefly, primers were designed to produce overlapping 1kb amplicons (Supplementary Table 1). Reverse transcriptase was performed as described in the ARTIC protocol. The single cDNA reaction was carried forward by preparing two PCR reactions, one each for the odd and even pools of primers. Two primer pools (odds and evens) were prepared to contain 0.1 µM of each individual primer. Tiling PCR of the resultant cDNA was performed by combining 12.5 µL 2x Q5 polymerase, 5.5 µL water, 2 µL of the primer pool, and 5 µL of cDNA followed by incubating the reaction at 98 °C for 30 seconds, 38 cycles of 98 °C for 15 seconds and 63 °C for 5 minutes, and holding at 4 °C. Corresponding odd and even amplicons were normalized and pooled for library preparation. Fragmented libraries were prepared using the Nextera XT DNA library preparation kit and sequenced via Illumina MiSeq. Analyses were performed using IRMA[25] with a SARS-CoV-2 module.

RNA extraction and RT-PCR

Preparation of viral RNA for next-generation sequencing was performed as described previously[10]. In brief, Vero E6 cells were infected with P.1 viruses. Extraction of total cellular RNA was done using Nucleospin® RNA Plus kit (Macherey-Nagel) according to the manufacturers' instruction.

RNA from hNE apical washes and mouse oropharyngeal swabs were prepared using QIAamp® Viral RNA Mini Kit (QIAGEN) and Nucleospin® RNA kit (Macherey-Nagel) according to the manufacturers' protocol.

To determine the ratios of S-614D:S-614G in competition assays in Epithelix and hACE2-KI mice, reverse transcription PCR was performed on extracted RNA using SuperScript™ IV One-step RT-PCR System (Invitrogen). The sequence-specific primers were used to generate an amplicon of 905 bp covering the D614G region: 5′-AATCTATCAGGCCGGTAGCAC-3′ and 5′-CAACAGCTATTCCAGTTAAAGCAC-3′. RT-PCR reaction was performed in a 50-µl reaction using 0.01 pg to 1µg total RNA. The cycling parameters were set as follows: 50°C for 10 min, 98°C for 2 min; 35 cycles at 98°C for 10 sec, 55°C for 15 sec, and 72°C for 30 sec; and a 5-min incubation at 72°C. DNA concentration was determined using Qubit dsDNA HS (High Sensitivity) Assay (Thermo Fisher), and subsequently diluted to 200 ng in 50 µL of nuclease-free water for sequencing by Nanopore sequencing MinION.

RNA extraction and preparation of RT-PCR reactions were performed in low- and no-copy laboratory environment to avoid contamination.

Sequencing and computational analysis

Recombinant SARS-CoV-2$^{S\text{-}614D}$ or SARS-CoV-2$^{S\text{-}614G}$ RNAs of P.1 stock were sequenced by next-generation sequencing as described previously[10]. Briefly, RNA was extracted from Vero E6 cells infected with either recombinant SARS-CoV-2$^{S\text{-}614D}$ or SARS-CoV-2$^{S\text{-}614G}$ using the NucleoSpin RNA Plus kit (Macherey-Nagel) according to the manufacturer's guidelines. Sequencing libraries were subsequently prepared using the Illumina TruSeq Stranded mRNA Library Prep kit (Illumina, 20020595) and pooled cDNA libraries were sequenced across two lanes on a NovaSeq 6000 S1 flow cell (2 x 50bp, 100 cycles) using the Illumina NovaSeq 6000 platform (Next Generation Sequencing Platform, University of Bern, Switzerland). For data analysis, TrimGalore v0.6.5 was used to remove low-quality reads and adaptors from the raw sequencing files. The resulting trimmed paired-end reads were then aligned to the SARS-CoV-2 genome (GenBank accession MT108784) using Bowtie2 v2.3.5. Finally, a consensus sequence was generated for each virus stock using Samtools v1.10 with the -d option set to 10,000. Data analysis was performed on UBELIX, the HPC cluster at the University of Bern (http://www.id.unibe.ch/hpc).

For virus competition experiments in hNE cells, hACE2-KI mice, hamsters, and ferrets, amplicons were sequenced on the MinION system from Oxford Nanopore. Real-time high accuracy basecalling, demultiplexing, and barcode and adapter trimming was performed with MinKnow v20.06.17, running Guppy vs4.0.11. Downstream analysis was done in Geneious 2019 vs2.3. Read length was filtered to eliminate reads < 800 and > 1100 nt and the remaining reads were mapped in subsets of 10,000 reads to the amplicon reference undergoing two iterations, with custom sensitivity allowing a maximum of 5% gaps and maximum mismatch 30%. Variants were analyzed at specific positions calculating p-values for each variant. Ratio fraction A/G was calculated from numbers of reads as fraction = Areads/(Areads+Greads).

Statistical analyses for virus competition experiments and relative replicative fitness calculations were performed using the catseyes package in R. Relative replicative fitness values for SARS-CoV-2$^{S\text{-}614G}$ over SARS-CoV-2$^{S\text{-}614D}$ were determined by dividing the initial SARS-CoV-2$^{S\text{-}614G}$/SARS-CoV-2$^{S\text{-}614D}$ ratio (i_0) by the final (post-infection) SARS-CoV-2$^{S\text{-}614G}$/SARS-CoV-2$^{S\text{-}614D}$ ratio (f_0) according to the formula $w = (f_0/i_0)$. Specifically, to model f_0/i_0 in each experiment, the T_1/T_0 ratio was calculated based on the sequencing counts attained for each virus in individual samples (post-infection time point T_1) and in the inoculum (initial time point T_0). For each time point, a linear regression model was generated in R and fitness ratios between the two groups (variants) were assessed by means of the coefficient of the model's Group term. When multiple experiments were performed, the Experiment variable was included in the model. All statistical tests were performed in R (R Core Team, 2020, v4.0.2) with two-sided alpha = 0.05. Cat's eye plots showing the relative replicative fitness of SARS-CoV-2$^{S\text{-}614G}$ over SARS-CoV-2$^{S\text{-}614D}$ for each time point in each experiment were created using the Catseyes package in R[26] as described in[20].

Animal studies

Ethics declarations. The hACE-2 knock-in mice were originally generated at the Wadsworth Center, New York State Department of Health IACUC protocol # 09-405 (Wentworth, PI). Mouse experimentation was conducted in compliance with the Swiss Animal Welfare legislation and animal studies were reviewed and approved by the commission for animal experiments of the canton of Bern, Switzerland under license BE-43/20. All of the ferret and hamster experiments were evaluated by the responsible ethics committee of the State Office of Agriculture, Food Safety, and Fishery in Mecklenburg-Western Pomerania, Germany (LALLF M-V), and gained governmental approval under registration number LVL MV TSD/7221.3-1- 041/20. This project also obtained clearance from the CDC's Animal Care and Use Program Office.

Human ACE2 knock-in mouse study. Generation of hACE2 knock-in mice. The hACE2-KI(B6) (B6.Cg-*Ace2*$^{tm1(ACE2)Dwnt}$/J) line was generated by targeted mutagenesis to express human ACE-2 cDNA in place of the mouse *Ace2* gene. Thus, in this new animal model, hACE2 expression is regulated by the endogenous mouse *Ace2* promoter/enhancer elements. The targeting vector (WEN1-HR) had hACE2 cDNA inserted in frame with the endogenous initiation codon of the mouse *Ace2* (Extended Data Figure 3a). The human cDNA was flanked by an FRT-neomycin-FRT-loxP cassette and a distal loxP site. WEN1-HR was used to transfect 129Sv/Pas ES cells and 837 ES cell clones were isolated and screened for homologous recombination by PCR and Southern blot. Eleven properly recombined ES cell clones were identified and some of them were used for blastocyst injection and implantation into female mice to generate 22 male founders with chimerism (129Sv/Pas:C57BL/6) ranging from 50 to 100%. To complete the hACE2 knock-in, we crossed the chimeric males with C57BL/6J Flp-expressing females to excise the FRT flanked neomycin selection cassette and generate the floxed humanised ACE2 allele (Extended Data Figure 3a). These hACE2 knock-in mice were identified by PCR and confirmed by Southern Blot and were backcrossed to C57BL/6J mice for 7 generations (N7) prior to this study. This line has been donated to The Jackson Laboratory for use by the scientific community (Stock 035000).

Heterozygous hACE2-KI female mice were obtained from The Jackson Laboratory (USA) and C57BL/6J wild-type (WT) female mice were from Janvier Lab (France). All mice were acclimatized for at least 2 weeks in individually ventilated cages (blue line, Tecniplast), with 12/12 light/dark cycle, 22±1 °C ambient temperature and 50±5% humidity, autoclaved acidified water, autoclaved cages including food, bedding, and environmental enrichment at the SPF facility of the Institute of Virology and Immunology, Mittelhäusern, Switzerland. One week before infection, mice were placed in individually HEPA-filtered isolators (IsoCage N, Tecniplast). Mice (10-12-week-old) were anesthetized with isoflurane and infected intranasally with 20 µL (*i.e.*, 10 µL per nostril) with a 1:1 ratio of the SARS-CoV-2 variants (WT and hACE2-KI mice) or mock culture medium (WT mice only). After intranasal infection, mice were monitored daily for body weight loss and clinical signs. Throat swabs were collected daily under brief isoflurane anesthesia using ultrafine sterile flock swabs (Hydraflock, Puritan, 25-3318-H). The tips of the swabs were place in 0.5 mL of RA1 lysis buffer (Macherey-Nagel, Ref. 740961) supplemented with 1% β-mercaptoethanol and vortexed. Groups of mice from two independent experiments were euthanized on days 2 and 4 p.i. and organs were aseptically dissected avoiding cross-contamination. Systematic tissue sampling was performed: (1) lung right superior lobe, right nasal concha, right olfactory bulb, part of the right brain hemisphere, apical part of the right kidney, parts of the distal small intestine (ileum) were collected for RNA isolation in RA1 lysis buffer; (2) lung middle, inferior and post-caval lobes, left nasal concha, left olfactory bulb, part of the right brain hemisphere, part of the right kidney were collected in MEM; (3) lung left lobe, liver left lobe, left kidney, left brain hemisphere and part of the jejunum and ileum were fixed in buffered formalin. Data were generated from two identically designed independent experiments.

Mouse tissue samples collected in RA1 lysis buffer supplemented with 1% β-mercaptoethanol were homogenized using a Bullet Blender Tissue Homogenizer (Next-Advance). Homogenates were centrifuged for 3 min at 18,000 g and stored at -70 °C until processing. Total RNA was extracted from homogenates using the NucleoMag VET kit for viral and bacterial RNA/DNA from veterinary samples (Macherey Nagel, Ref: 744200) and the KingFisher Flex automated extraction instrument (ThermoFisher Scientific) following manufacturers' instructions. RNA purity was analyzed with a NanoDrop 2000 (ThermoFisher Scientific). A 25 µL RT-PCR for the viral E gene was carried out using 5 µL of extracted RNA template using the AgPath-ID One-Step RT-PCR (Applied Biosystems). Samples were processed in duplicate. Amplification and detection were performed in an Applied Biosystem 7500 Real-Time PCR Systems under the following conditions: an initial reverse transcription at 45 °C for 10 min, followed by PCR activation at 95 °C for 10 min and 45 cycles of amplification (15 seconds at 95 °C, 30 seconds at 56 °C and 30 seconds at 72 °C).

Fixed mouse tissue samples were processed, sectioned, and stained with hematoxylin and eosin (H&E) at the COMPATH core facility (University of Bern). Histopathological lung slides of hACE2-KI mice and wild-type mice (infected and mock) were examined and scored by a board-certified veterinary pathologist (SdB), who was blinded to the identity of the samples. Scoring criteria are detailed in Extended Data Table 2.

Hamster study. Six Syrian hamsters, *Mesocricretus auratus*, (Janvier Labs, France) were infected intranasally under a short-term inhalation anesthesia with 70 µl of SARS-CoV-$2^{S\text{-}614D}$ and SARS-CoV-$2^{S\text{-}614G}$ at equal ratios using $10^{4.77}$ $TCID_{50}$/animal (calculated from back titration of the original material). After 24 hours of isolated housing in individually ventilated cages (IVCs), six pairs, each with one directly inoculated donor hamster and one sham-inoculated contact hamster were co-housed. The housing of each hamster duo was strictly separated in individual cage systems to prevent spill-over between different pairs. For the following seven days (day 2 until day 8 after infection) and on day 12 after infection, viral shedding was monitored in addition to a daily physical examination and body weighting routine.

To evaluate viral shedding, nasal washes were individually collected from each hamster under a short-term isoflurane anesthesia. Starting with the pair's contact hamster, each nostril was rinsed with 100 µl PBS (1.0x phosphate-buffered saline) and reflux was immediately gathered. A new pipet tip for every nostril and hamster was used to prevent indirect spill-over transmission from one animal to another. Furthermore, in-between the respective pairs, a new anesthesia system was used for each pair of animals. At day 8 post infection, one contact hamster was found dead. Although having lost up to almost 20% of their body weight, every other hamster recovered from disease. Under euthanasia, serum samples were collected from each hamster.

For the single-virus infection experimental setup seven hamsters each were infected via the intranasal route with $10^{5.1}$ $TCID_{50}$/animal of SARS-CoV-$2^{S\text{-}614D}$, or $10^{4.5}$ $TCID_{50}$/animal SARS-CoV-$2^{S\text{-}614G}$ (calculated from back titration of the original material). From day 1 onwards to day 4 nasal washes were obtained from these hamsters and body weight changes recorded. A tissue panel from respiratory organs, including nasal conchae, tracheal tissue, cranial, medial, and caudal portions of the right lung, and the pulmonary lymph node, were collected after euthanasia from these hamsters.

Ferret study. In accordance with the hamster study, twelve ferrets (*Mustela putorius furo*) from in-house breeding, were divided into six groups of two individuals. Ferret pairs were of equal age between four and 18 months. In total, four ferrets were female (two pairs) and eight ferrets were male or neutered male (four pairs). The housing of each ferret duo was strictly separated in individual cage systems, to prevent spill-over between different pairs. Per separate cage, one individual ferret was inoculated intranasally, by instillation of 125µl of the aforementioned inoculum ($1x10^5$ $TCID_{50}$/animal; calculated from back titration of the original material) into each nostril under a short-term isoflurane-based inhalation anesthesia. Time points and sampling technique corresponded to the methods used for the hamsters, albeit ferret nasal washing was performed using two times 700µl PBS per animal. The contact-ferret was not inoculated.

Specimen work-up, viral RNA detection, sequencing and quantification analyses. Organ samples were homogenized in a 1 ml mixture of equal volumes composed of Hank's balanced salts minimum essential medium (MEM) and Earle's balanced salts MEM containing 2 mM l-glutamine, 850 mg l−1 NaHCO3, 120 mg l−1 sodium pyruvate and 10% FCS (supplemented with 10% Fetal Calf Serum and 1% penicillin–streptomycin) at 300 Hz for two minutes using the Tissuelyser II (Qiagen, Hilden, Germany) and centrifuged to clarify the supernatant. Nucleic acid was extracted from 100 µl of the nasal washes after a short centrifugation step or organ sample supernatant using the NucleoMag Vet kit (Macherey Nagel, Düren, Germany). Viral loads in these samples were determined using the nCoV_IP4 RT-PCR[28] including standard RNAs that where absolute quantified by digital droplet PCR with a sensitivity of 10 copies/reaction. The extracted RNA was afterwards subjected to MinION sequencing and digital droplet PCR. For MinION sequencing, amplicons were produced with primers (WU-21-F: AATCTATCA GGCCGGTAGCAC; WU-86-R: CAACAGCTATTCCAGTTAAAGCAC) using SuperScript IV One-step RT-PCR (Thermo Fisher Scientific; Waltham, MA USA). Amplicons were sequenced on a MinION system using from Oxford Nanopore using Native Barcoding 1-12 (EXP-NBD104) and 13-24 (EXP-NBD114), respectively with Ligation Kit SQK-LSK109 (Oxford Nanopore; Oxford, UK). Libraries were loaded on R9.4.1 Flow Cells (FLO-MIN106D) on a MinION coupled to a MinIT. MinION data analysis was performed as previously described in the sequencing and computational analysis section above.

For rare mutation and sequence analysis based on digital PCR, the QX200 Droplet Digital PCR System from Bio-Rad (Hercules, CA, USA)

was used. For RT-PCR, the One-Step RT-ddPCR Advanced Kit for Probes (Bio-Rad) was applied according to the supplier´s instructions. For the amplification of an 86 bp fragment of both variants of the spike protein gene, the forward primer SARS2-S-1804-F (5´-ACA AAT ACT TCT AAC CAG GTT GC-3´) and the reverse primer SARS2-S-1889-R (5´-GTA AGT TGA TCT GCA TGA ATA GC-3´) were used. For the detection of the D and G variants in one sample, two allele specific locked nucleic acid (LNA) probes were applied: SARS2-S-v1D-1834FAM (5´-FAM-TaT cAG gat GTt AAC-BHQ1-3´) and SARS2-S-v3G-1834HEX (5´-HEX-T cAG ggt GTt AAC-BHQ1-3´). The LNA positions are depicted in lower case. The concentration of the primers and probes was 20µM and 5µM, respectively. For data analysis, the QuantaSoft Analysis Pro software (version 1.0.596) was used.

Reporting summary

Further information on research design is available in the Nature Research Reporting Summary linked to this paper.

Data availability

Sequence data are available on the NCBI Sequence Read Archive (SRA) under the BioProject accession number PRJNA669553. Source data are provided with this paper.

23. van den Worm, S.H. et al. Reverse genetics of SARS-related coronavirus using vaccinia virus-based recombination. *PLoS One* **7**, e32857 (2012).
24. Thiel, V., Herold, J., Schelle, B. & Siddell, S.G. Infectious RNA transcribed in vitro from a cDNA copy of the human coronavirus genome cloned in vaccinia virus. *J Gen Virol* **82**, 1273-1281 (2001).
25. Shepard, S.S. et al. Viral deep sequencing needs an adaptive approach: IRMA, the iterative refinement meta-assembler. *BMC Genomics* **17**, 708 (2016).
26. Anderson, C. (2019). Catseyes: create catseye plots illustrating the normal distribution of the means (R Package version 0.2.3).

Acknowledgements This work was supported by the Swiss National Science Foundation (SNF; grants 31CA30_196644, 31CA30_196062, and 310030_173085), the European Commission (Marie Skłodowska-Curie Innovative Training Network "HONOURS"; grant agreement No. 721367, and the Horizon 2020 project "VEO" grant agreement No. 874735), the Federal Ministry of Education and Research (BMBF; grant RAPID, #01KI1723A) and by core funds of the University of Bern and the German Federal Ministry of Food and Agriculture. The hACE2-KI(B6) KI mice were generated with support from NIH/NIAID P01AI059576 (subproject 5) and partial support from NIH/NIAID U54-AI-057158. Partial support was from the US Centers for Disease Control and Prevention COVID-19 Task Force. We thank the NGS platform of the University of Bern. We also acknowledge Mareen Lange, Christian Korthase, Michael Currier and Gloria Larson and Sandra Renzullo for their excellent technical assistance and Frank Klipp, Doreen Fiedler, Harald Manthei, Christian Lipinski, Jianzhong Tang, and Aurélie Godel for their invaluable support in the animal experiments. This activity was reviewed by CDC and was conducted consistent with applicable federal law and CDC policy: 45 C.F.R. part 46, 21 C.F.R. part 56; 42 U.S.C. Sect. 241(d); 5 U.S.C. Sect. 552a; 44 U.S.C. Sect. 3501 et seq. The findings and conclusions in this manuscript are those of the authors and do not necessarily represent the official position of the US Centers for Disease Control and Prevention.

Author contributions VT, DW, MB, and CB conceived the study. TT, BZ, DH, AT performed most of the experiments. NE, SS, FL, JKe, HS, JP, HS, BT, JJ, RD, DH, NJH, LU, JKi, AP, BH, XF, XL, LW, NJ, DC, JH, MW, MK, TS, JR, SdB, CB conducted experimental work and/or provided essential experimental systems, data analysis, and reagents. VT, DW, MB, CB, TT, BZ, NE, SS, LT, DH, NJH, LU wrote the manuscript and made the figures. All authors read and approved the final manuscript.

Competing interests The authors declare no competing interests.

Additional information

Supplementary information The online version contains supplementary material available at https://doi.org/10.1038/s41586-021-03361-1.

Correspondence and requests for materials should be addressed to V.T., M.B., D.E.W. or C.B.

Peer review information *Nature* thanks Stanley Perlman and the other, anonymous, reviewer(s) for their contribution to the peer review of this work.

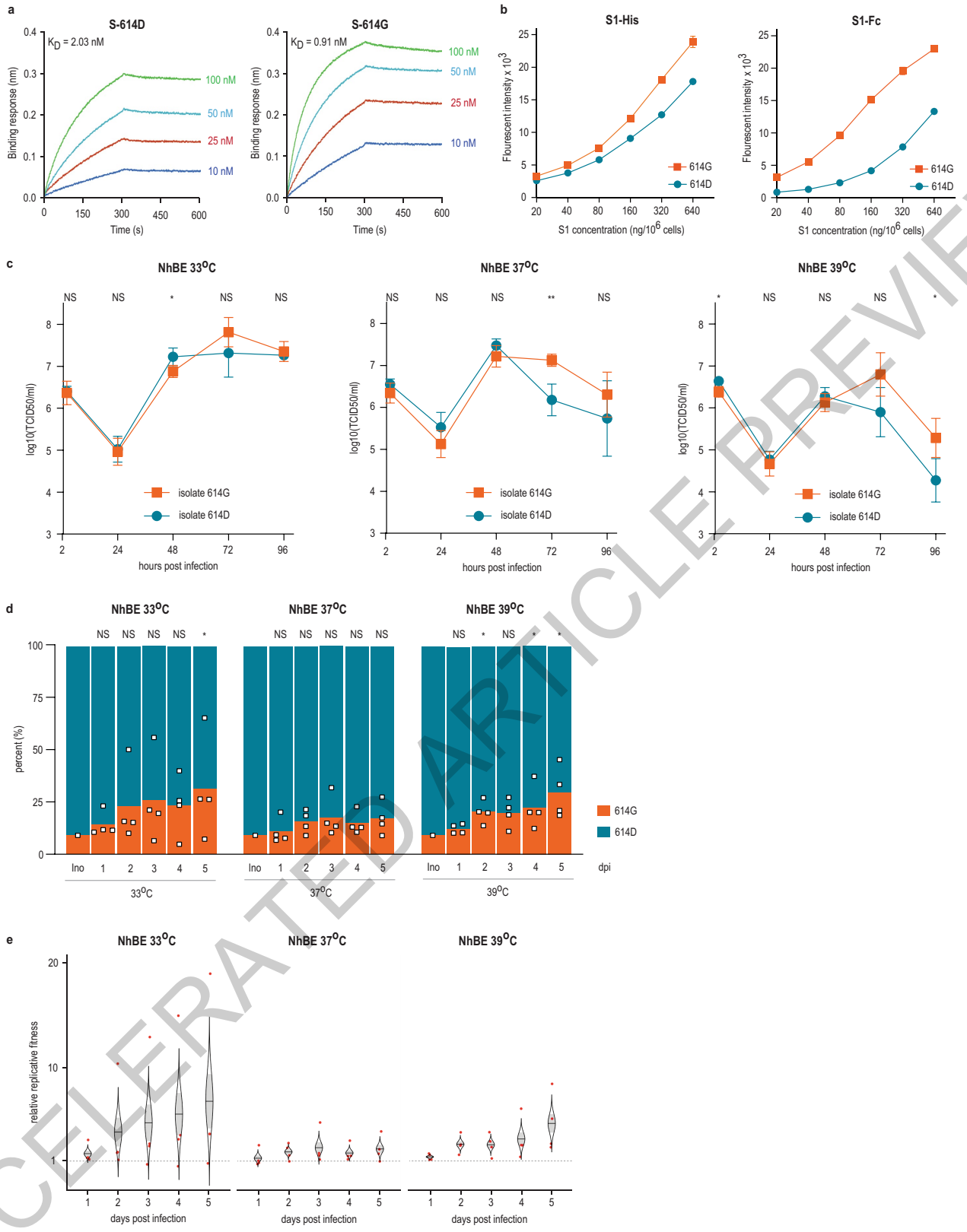

Extended Data Fig. 1 | See next page for caption.

Extended Data Fig. 1 | Additional *in vitro* characterization of S proteins and SARS-CoV-2$^{S\text{-}614D}$ and SARS-CoV-2$^{S\text{-}614G}$ isolates. **(a)** Affinity between S and hACE2 determined by Bio-layer interferometry. Fc-tagged hACE2 was loaded onto surface of AHC biosensors and association was conducted using S-614D or S-614G followed by dissociation. Data represent three biological replicates and all repeats with statistical analysis were provided in Supplementary Table 2. **(b)** Binding of polyhistidine-tagged or Fc-tagged S1 to BHK-hACE2 cells determined by flow cytometry. Mean Fluorescence intensity is shown for corresponding S1 protein concentration. Data represent the mean ± s.d of three biological replicates. **(c)** Replication of wild type SARS-CoV-2/USA-WA1/2020 (S-614D) and SARS-CoV-2/Massachusetts/VPT1/2020 (S-614G) isolates in NhBE cells at 33°C (left), 37°C (middle), and 39°C (right). NhBE cells were infected with 200,000 TCID50 of each virus. Supernatants were collected every 24 h and titrated by TCID50 assay. Data represent the mean ± s.d. of four replicates. Statistical significance was determined by two-sided unpaired Student's *t*-test without adjustments for multiple comparisons. *P* values (from left to right): left, NS $P = 0.8098$; NS $P = 0.7874$; $^{*}P = 0.0328$; NS $P = 0.1887$; NS $P = 0.5296$; middle, NS $P = 0.1689$; NS $P = 0.1475$; NS $P = 0.1415$; $^{**}P = 0.0033$; NS $P = 0.3184$; right, $^{*}P = 0.0197$; NS $P = 0.6018$; NS $P = 0.3903$; NS $P = 0.0898$; $^{*}P = 0.0445$. **(d)** Competition assay of recombinant SARS-CoV-2$^{S\text{-}614D}$ and SARS-CoV-2$^{S\text{-}614G}$ in NhBE at 33°C, 37°C and 39°C. The inoculum was prepared by mixing two viruses at 9:1 ratio based on plaque forming unit ml^{-1}. NhBE was infected with 100,000 pfu of the 9:1 virus mix (n=4). Viral RNA was extracted from daily supernatant and sequenced by next generation sequencing. Percentage of sequencing reads encoding either S-614D or S-614G. Each square represents one individual data point in competition experiment. For each time point, a linear regression model was generated based on the sequence read counts for S-614D and S.614G, and *P* values were calculated for the group (variant) coefficient. *P* values (left to right): left, NS $P = 0.1796$; NS $P = 0.087$ NS $P = 0.1147$; NS $P = 0.1244$; $^{*}P = 0.0401$; middle, NS $P = 0.9114$; NS $P = 0.0715$; NS $P = 0.1696$; NS $P = 0.1696$; NS $P = 0.1657$; right, NS $P = 0.1041$; $^{*}P = 0.013$; NS $P = 0.0645$; NS $^{*} = 0.0102$; $^{*}P = 0.0308$. **(e)** Cat's eye plot illustrating the relative replicative fitness values of S-614G over S-614D in NhBE cells for the competition experiments performed in **(d)**. Each dot represents an individual data point, the centerline represents the mean, and the shaded area represents the standard deviation.

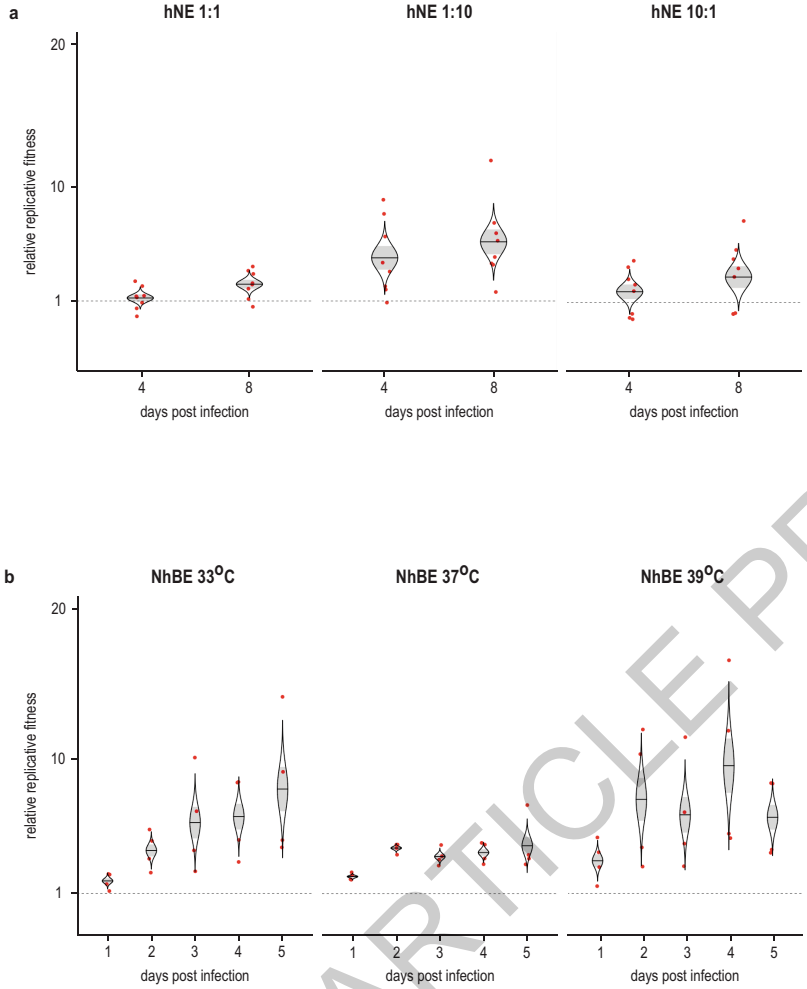

Extended Data Fig. 2 | Cat's eye plots illustrating the relative replicative fitness values of S-614D over S-614G in hNE (a) and NhBE (b) for the competition experiments shown in Fig 1e and Fig 1f. Each dot represents an individual data point, the centre line represents the mean, and the shaded area represents the standard deviation.

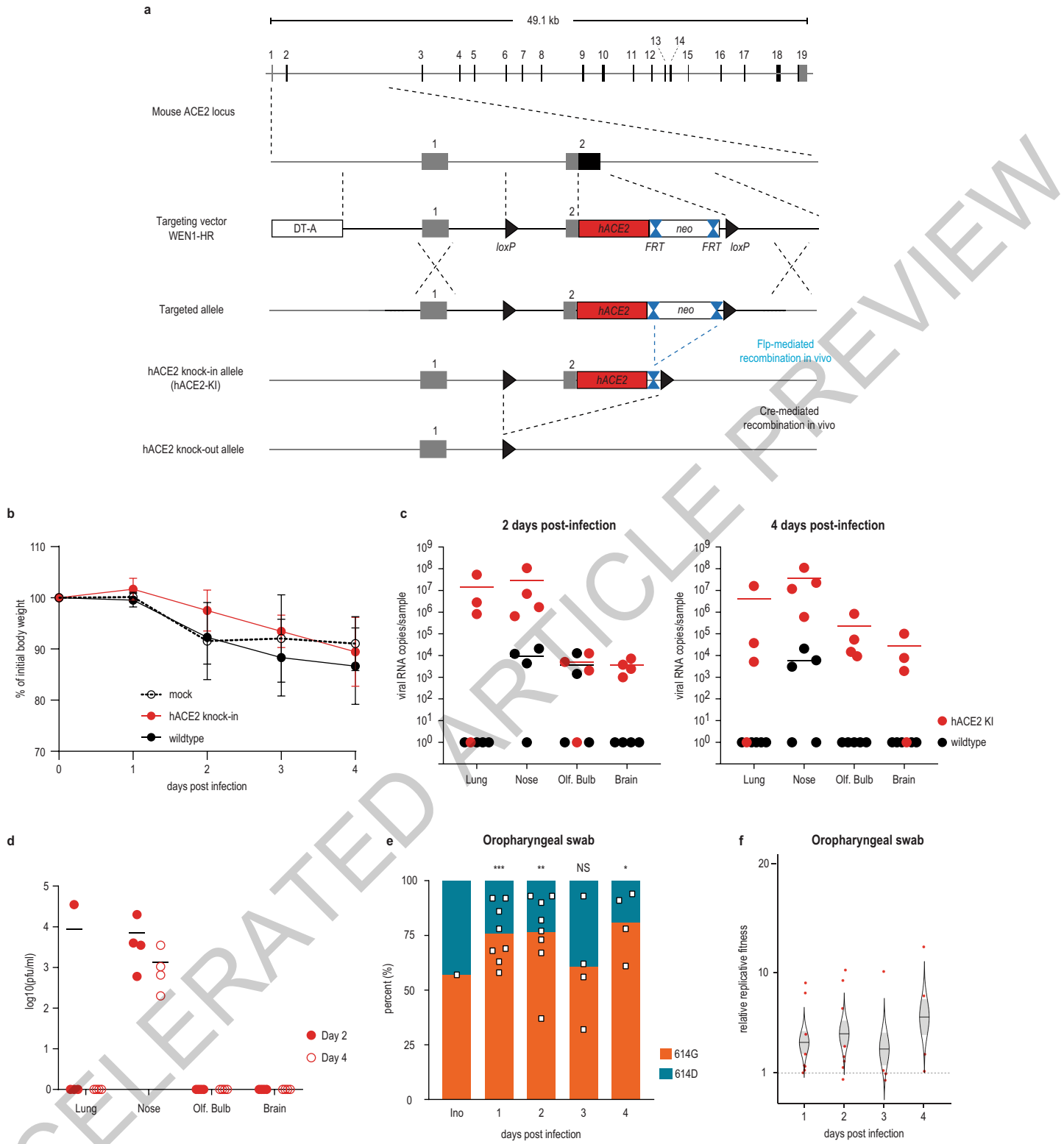

Extended Data Fig. 3 | See next page for caption.

Extended Data Fig. 3 | hACE-2 KI mouse generation and infection with SARS-CoV-2$^{S\text{-}614D}$ and SARS-CoV-2$^{S\text{-}614G}$ viruses. (**a**) Design and generation of humanized ACE2 knock-in mice (hACE2-KI). The hACE2 cDNA was inserted in frame with the endogenous initiation codon of mouse *Ace2* in exon 2, which was deleted. The hACE2 cDNA was flanked 5′ with a loxP site (black triangle) and 3′ with a FRT-neomycin-FRT-loxP cassette. The targeting construct included a negative selection cassette (PGK-DTA) to improve selection of clones with homologous recombination. Chimeric male mice transmitting the targeted locus were crossed with Flp-deleter female mice to generate the floxed hACE2 knock-in allele. This allele can be used : (1) without further cre-mediated recombination, as shown here, to study humanized ACE2 mice (hACE2-KI), where the hACE2 cDNA is expressed in place of mouse Ace2; (2) after crossing with a cre-deleter mouse line to generate constitutive *Ace2* knock-out mice; (3) after crossing with tissue-specific cre line. Ubiquitous and tissue-specific knock-out mice can be crossed with conventional hACE2 transgenic mice to remove the endogenous mouse ACE2, which could confound pathogenesis studies that may occur due to heterodimerization of ACE2. (**b**) Body weight loss at indicated time points after infection of hACE2-KI mice (n=8), wild-type mice infected (n=9) and for mock-infected wild-type sampled identically (n=10). (**c,d**) Quantitative RT-PCR analysis **(c)** and viral titers **(d)** of tissue homogenates of inoculated hACE2-KI and wild-type mice at indicated time points. (**e**) Percentage of sequencing reads encoding either S-614D or S-614G. Each square represents data for one individual mouse in competition experiment. For each time point, a linear regression model was generated based on the sequence read counts for S-614D and S-614G, and *P* values were calculated for the group (variant) coefficient. *P* values (left to right): *** $P = 0.0009$; ** $P = 0.0020$; NS $P = 0.7875$; * $P = 0.0180$. (**f**) Cat's eye plot illustrating the relative replicative fitness values of S-614D over S-614G from oropharyngeal swabs of hACE2-KI in competition experiment performed in Fig 2. Ratios of S-614G over S-614D were measured after competition using the MinION sequencing platform at the time point indicated on the plot. Each dot represents one infected hACE2-KI mouse, the centre line represents the mean, and the shaded area represents the standard deviation.

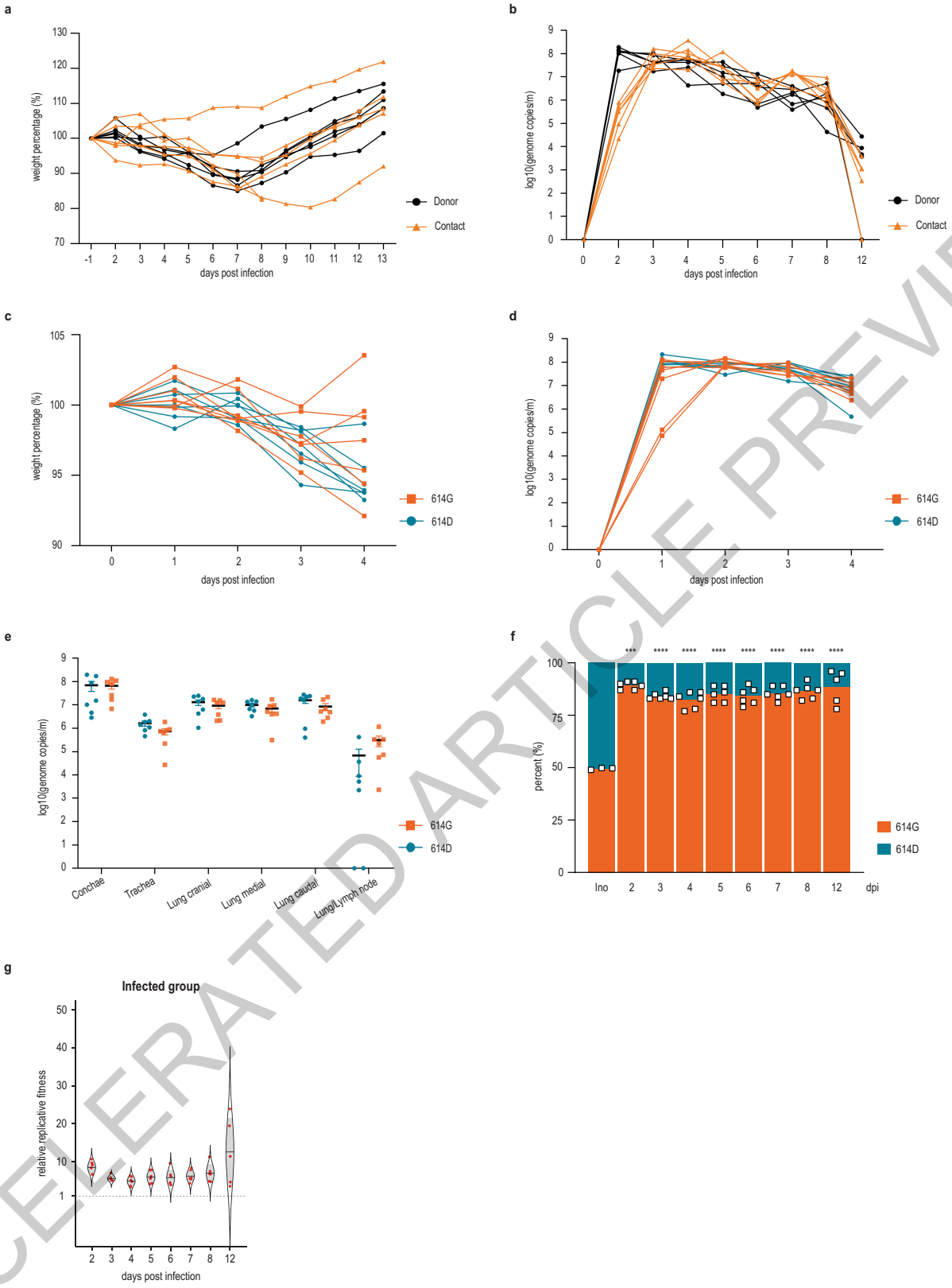

Extended Data Fig. 4 | See next page for caption.

Extended Data Fig. 4 | Virus replication in infected Syrian hamsters. (a) Body weight loss at indicated time points after infection of Syrian hamsters. Donor animals (n=6; black dots) were intranasally inoculated with SARS-CoV-$2^{S\text{-}614D}$ / SARS-CoV-$2^{S\text{-}614G}$ at equal ratio ($1x10^{4.77}$ $TCID_{50}$/animal as determined by back-titration of the original inoculum). 24h after infection, naïve hamsters (n=6; orange triangles) were housed in direct contact in an "one-to-one" experimental setup. **(b)** Quantitative RT-PCR analysis of individual nasal washing samples obtained from donor hamsters and contact animals, respectively. **(c)** Body weight loss at the indicated time points after infection of the hamsters. Syrian hamsters were inoculated with $10^{5.1}$ $TCID_{50}$/animal of SARS-CoV-$2^{S\text{-}614D}$ (n=7, blue dots), or $10^{4.5}$ $TCID_{50}$/animal SARS-CoV-$2^{S\text{-}614G}$ (n=7, red triangles) via the intranasal route. Titers were determined by backtitration of the original inoculation material. **(d)** Viral genome copy numbers are shown as determined by RT-qPCR from individual nasal washing samples of the animals inoculated with the single variant virus. **(e)** Quantitative RT-PCR analysis of tissue homogenates of inoculated hamsters of the SARS-CoV-$2^{S\text{-}614D}$ group (n=7, blue dots) versus the SARS-CoV-$2^{S\text{-}614G}$ group (n=7, red triangles). **(f)** Percentage of sequencing reads encoding either S-614D or S-614G. Each square represents data for one individual hamster in competition experiment. For each time point, a linear regression model was generated based on the sequencing read counts for S-614D and S-614G, and *P* values were calculated for the group (variant) coefficient. *P* values (left to right): *** $P = 0.0007$; **** $P < 0.0001$. **(g)** Cat's eye plot showing the relative repicative fitness values of S-614G over S-614D for infected hamsters from the competition experiment performed in Fig 3. Ratios of S-614G over S-614D were measured after competition using the MinION sequencing platform at the time points indicated on the plot. Each dot represents one infected animal (n = 6), the centre line represents the mean, and the shaded area represents the standard deviation.

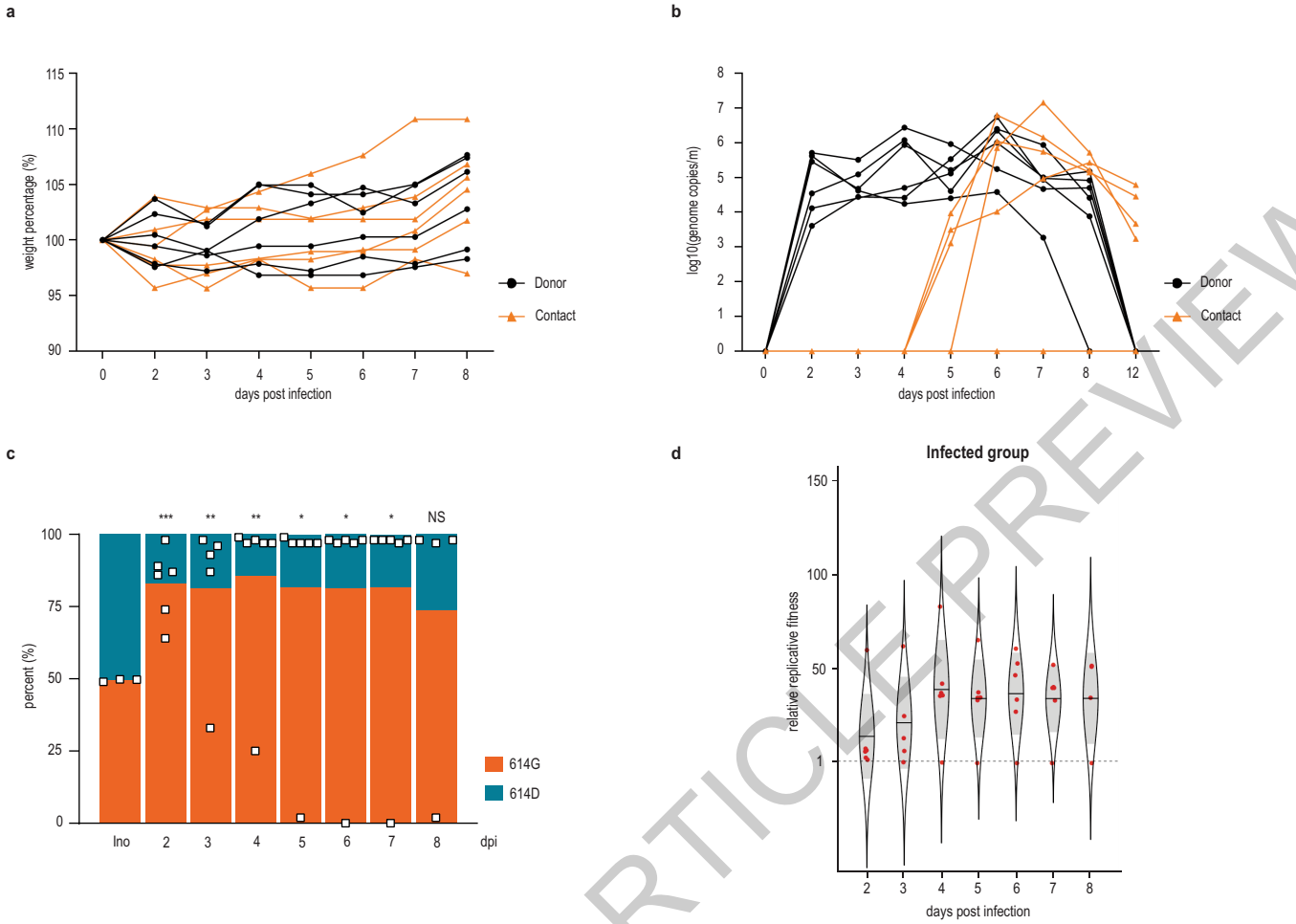

Extended Data Fig. 5 | "Twin"-inoculation of donor ferrets with equal ratios of SARS-CoV-2$^{S\text{-}614D}$ and SARS-CoV-2$^{S\text{-}614G}$. Donor ferrets (black dot; n=6) were intranasally inoculated with $10^{5.4}$ $TCID_{50}$/animal as determined by back titration of an inoculum comprising equal ratios of SARS-CoV-2$^{S\text{-}614D}$ and SARS-CoV-2$^{S\text{-}614G}$. Twenty-four hours post inoculation one contact ferret (orange triangle; n=6) was commingled with one donor ferret, creating six donor – contact ferret pairs. **(a)** Individual body weight of ferrets at the indicated days, relative to the day of inoculation, is plotted. **(b)** Genome copy numbers for inoculated donor and contact ferrets. Individual nasal washing samples of the indicated days were analyzed by RT-qPCR "nCoV_IP4", and absolute numbers were calculated using a set of standard RNAs. All donor ferrets (black dots) tested vRNA positive, starting already day 2 post inoculation (n=6). 4 out of 6 contact ferrets (orange triangles) tested vRNA positive beginning with day 4 (corresponding with day 3 after contact). 2 of the 6 contact ferrets never tested positive for vRNA throughout the study. **(c)** Percentage of sequencing reads encoding either S-614D or S-614G. Each square represents data for one individual ferret in competition experiment. Statistical significance was determined by Fisher's exact test. *** *P* values (left to right): *** $P = 0.0001$; ** $P = 0.0090$; ** $P = 0.0030$; * $P = 0.0352$; * $P = 0.0393$; * $P = 0.0411$; NS $P = 0.2883$. **(d)** Cat's eye plot illustrating the relative replicative fitness values of S-614G over S-614D in infected ferrets from the competition experiment performed in Fig 4. Ratios of S-614G over S-614D were measured after competition using the MinION sequencing platform at the time points indicated on the plot. Each dot represents one infected ferret (n = 6), the centre line represents the mean, and the shaded area represents the standard deviation.

nature research

Corresponding author(s): Thiel, Beer, Wentworth, Benarafa

Last updated by author(s): 2020/12/14

Reporting Summary

Nature Research wishes to improve the reproducibility of the work that we publish. This form provides structure for consistency and transparency in reporting. For further information on Nature Research policies, see Authors & Referees and the Editorial Policy Checklist.

Statistics

For all statistical analyses, confirm that the following items are present in the figure legend, table legend, main text, or Methods section.

n/a	Confirmed
☐	☒ The exact sample size (*n*) for each experimental group/condition, given as a discrete number and unit of measurement
☐	☒ A statement on whether measurements were taken from distinct samples or whether the same sample was measured repeatedly
☐	☒ The statistical test(s) used AND whether they are one- or two-sided *Only common tests should be described solely by name; describe more complex techniques in the Methods section.*
☒	☐ A description of all covariates tested
☐	☒ A description of any assumptions or corrections, such as tests of normality and adjustment for multiple comparisons
☐	☒ A full description of the statistical parameters including central tendency (e.g. means) or other basic estimates (e.g. regression coefficient) AND variation (e.g. standard deviation) or associated estimates of uncertainty (e.g. confidence intervals)
☐	☒ For null hypothesis testing, the test statistic (e.g. *F*, *t*, *r*) with confidence intervals, effect sizes, degrees of freedom and *P* value noted *Give P values as exact values whenever suitable.*
☒	☐ For Bayesian analysis, information on the choice of priors and Markov chain Monte Carlo settings
☒	☐ For hierarchical and complex designs, identification of the appropriate level for tests and full reporting of outcomes
☒	☐ Estimates of effect sizes (e.g. Cohen's *d*, Pearson's *r*), indicating how they were calculated

Our web collection on statistics for biologists contains articles on many of the points above.

Software and code

Policy information about availability of computer code

Data collection	Data acquisition for Minion sequencing was done with MinKNOW version 20.06.17 and basecalling software Guppy version 4.0.11
Data analysis	seqeunce analysis: Geneious Prime ® 2019.2.3 virus kinetics analyses: GraphPad Prism version 8.3.0 for Windows figures: Adobe Illustrator CS6; Catseyes version 0.2.5; R version 4.0.2 NGS (RNAseq): TrimGalore software (version 0.6.5), SAMtools (version 1.10); Bowtie2 version 2.3.5 Minion sequencing: MinKnow version 20.06.17; Guppy version 4.0.11 digital PCR: QuantaSoft Analysis Pro software (version 1.0.596) FACS: Flowjo_v10.6.1.

For manuscripts utilizing custom algorithms or software that are central to the research but not yet described in published literature, software must be made available to editors/reviewers. We strongly encourage code deposition in a community repository (e.g. GitHub). See the Nature Research guidelines for submitting code & software for further information.

Data

Policy information about availability of data

All manuscripts must include a data availability statement. This statement should provide the following information, where applicable:

- Accession codes, unique identifiers, or web links for publicly available datasets
- A list of figures that have associated raw data
- A description of any restrictions on data availability

Sequence data are available on the NCBI Sequence Read Archive (SRA) under the BioProject accession number PRJNA669553.

Field-specific reporting

Please select the one below that is the best fit for your research. If you are not sure, read the appropriate sections before making your selection.

☒ Life sciences ☐ Behavioural & social sciences ☐ Ecological, evolutionary & environmental sciences

For a reference copy of the document with all sections, see nature.com/documents/nr-reporting-summary-flat.pdf

Life sciences study design

All studies must disclose on these points even when the disclosure is negative.

Sample size	No sample size calculations were performed. Sample sizes were based on standards in the field, typically 3 independent biological replicates, with each replicate assayed in technical duplicate or triplicate. Experiments involving hNE and NhBE primary airway cultures were done in technical replicates since these cells are purchased and are delivered with a quality guarntee for the delivery data. Therefore only technical replicates were performed.
Data exclusions	no data was excluded
Replication	all attempts at replication were successful; experiments were performed according to best practices and as described in the methods.
Randomization	randomization was not applied since cloning procedures, virus infection/titrations, and inhibitor/neutralization experiments did not require randomization.
Blinding	blinding was done for seqeuncing analyses for the determination of the ratio of genotypes 614D vs 614G. For all other experiments blinding was not done.

Reporting for specific materials, systems and methods

We require information from authors about some types of materials, experimental systems and methods used in many studies. Here, indicate whether each material, system or method listed is relevant to your study. If you are not sure if a list item applies to your research, read the appropriate section before selecting a response.

Materials & experimental systems

n/a	Involved in the study
☐	☒ Antibodies
☐	☒ Eukaryotic cell lines
☒	☐ Palaeontology
☐	☒ Animals and other organisms
☒	☐ Human research participants
☒	☐ Clinical data

Methods

n/a	Involved in the study
☒	☐ ChIP-seq
☐	☒ Flow cytometry
☒	☐ MRI-based neuroimaging

Antibodies

Antibodies used	Goat anti-Human IgG (H+L) Cross-Adsorbed Secondary Antibody, Alexa Fluor 633, 1:300 dilution (ThermoFisher Cat # A-21091 for Fc tag) 6x-His Tag Monoclonal Antibody (HIS.H8), Alexa Fluor 647, 1:300 dilution (ThermoFisher Cat # MA1-21315-647 for polyhistidine-tag)
Validation	No primary antibodies were used in this study. The only things that are “similar to” primary antibodies are His-tagged or Fc-tagged S1 proteins for hACE2 detection in FACS, which were validated by BLI assay and ELISA assay so confirm they can bind to hACE2.

Eukaryotic cell lines

Policy information about cell lines

Cell line source(s)	VeroE6 (obtained from Marcel Müller, Charité, Berlin) BHK-SARS-N (prepared and published in: van den Worm, S. H. et al. Reverse genetics of SARS-related coronavirus using vaccinia virus-based recombination. PLoS One 7, e32857, doi:PONE-D-11-21011) BHK-hACE2 (perpared in this study)

Authentication	Profiling of cell line was done using highly-polymorphic short tandem repeat loci (STRs). Fragment analysis was done on an ABI3730xl (Life Technologies) and the resulting data were analyzed with GeneMarker software (Softgenetics).
Mycoplasma contamination	all cell lines in our laboratories are routinely screened for micoplasma contamination and were tested negative.
Commonly misidentified lines (See ICLAC register)	none

Animals and other organisms

Policy information about studies involving animals; ARRIVE guidelines recommended for reporting animal research

Laboratory animals	Mice. 10-12 weeks old. Female heterozygous Ace2<tm1(ACE2)Dwnt>/J mice were used. They were housed at 22°C ambient temperature and 50% humidity. Detailed experimentation protocols and are fully disclosed according the ARRIVE guidlines in the methods' section of the manuscript. Ferrets. 4-9 months old ferrets (Mustela putorius furo, 4 female and 8 male) were infected intranasally with the indicated viruses. They were housed at 22°C ambient temperature and 50% humidity. Hamsters. 8 weeks old Syrian hamsters (Mesocricretus auratus, 26 male) were infected intranasally with the indicated viruses. They were housed at 22°C ambient temperature and 50% humidity.
Wild animals	no wild animals were used in the study.
Field-collected samples	no field collected samples were used in the study.
Ethics oversight	Mice. The hACE-2 knock-in mice (B6.129S2(Cg)-Ace2<tm1(ACE2)Dwnt>/J) were originally generated at the Wadsworth Center, New York State Department of Health IACUC protocol # 09-405 (Wentworth, PI). Mouse experimentation was conducted at the Institute of Virology and Immunology, Mittelhäusern, Switzerland in compliance with the Swiss Animal Welfare legislation and animal studies were reviewed and approved by the commission for animal experiments of the canton of Bern, Switzerland under license BE-43/20. Ferrets and hamsters. All ferret and hamster experiments were evaluated by the responsible ethics committee of the State Office of Agriculture, Food Safety, and Fishery in Mecklenburg-Western Pomerania, Germany (LALLF M-V), and gained governmental approval under registration number LVL MV TSD/7221.3-1- 041/20.

Note that full information on the approval of the study protocol must also be provided in the manuscript.

Flow Cytometry

Plots

Confirm that:

☒ The axis labels state the marker and fluorochrome used (e.g. CD4-FITC).

☒ The axis scales are clearly visible. Include numbers along axes only for bottom left plot of group (a 'group' is an analysis of identical markers).

☒ All plots are contour plots with outliers or pseudocolor plots.

☒ A numerical value for number of cells or percentage (with statistics) is provided.

Methodology

Sample preparation	BHK cells expressing exogenous hACE2 were pelleted and resuspended in reaction buffer (PBS pH7.4, 0.02% tween20, BSA 4%) at a concentration of 5 × 106 cells/ml. 100 ul/well of the cells were aliquoted into a round-bottom 96-well plate and incubated on ice for at least 5 min. S1 proteins were diluted in reaction buffer on ice. 50ul of S1 diluents were added into corresponding wells of cells and incubated on ice for 20 min with shaking. After incubation, cells were washed in 200ul washing solution (PBS pH7.4, 0.02% tween 20) once and then 100ul of 1:300 diluted secondary antibody (ThermoFisher Cat # A-21091 for Fc tag and ThermoFisher Cat # MA1-21315-647 for polyhistidine-tag) was added into each well of cells, mixed, and incubated on ice with shaking for 15 min. After washing twice, cells were resuspended in 200ul PBST and analyzed using the BD FACSCanto II Flow Cytometer. Data was processed with Flowjo_v10.6.1.
Instrument	BD FACSCanto II Flow Cytometer
Software	Flowjo_v10.6.1.
Cell population abundance	BHK cells expressing hACE2 were used as the only cell population
Gating strategy	BHK cells expressing hACE2 were used without S1Fc or S1-His and mean fluorescence intesity was measured in comparison with BHK cells expressing hACE2 incubated with indicated concentrations of S1-Fc or S1-His. Shifts in mean fluorescence intensity were recoreded and displayed in Fig 1b and Extended Data Figure 1b.

☒ Tick this box to confirm that a figure exemplifying the gating strategy is provided in the Supplementary Information.